Engineering NIR-Sighted Bacteria

Stefanie S. M. Meier[1,‡], Michael Hörzing[1,‡], Cornelia Böhm[2,3,‡], Emma L. R. Düthorn[1,‡], Heikki Takala[2,‡], René Uebe[4,5,‡], Andreas Möglich[1,5,6,*,‡]

[1] Department of Biochemistry, University of Bayreuth, 95447 Bayreuth, Germany.
[2] Department of Biological and Environmental Science, Nanoscience Center, University of Jyvaskyla, Jyvaskyla 40014, Finland.
[3] Institute of Biochemistry, Graz University of Technology, 8010 Graz, Austria
[4] Department of Microbiology, University of Bayreuth, 95447 Bayreuth, Germany.
[5] Bayreuth Center for Biochemistry & Molecular Biology, Universität Bayreuth, 95447 Bayreuth, Germany.
[6] North-Bavarian NMR Center, Universität Bayreuth, 95447 Bayreuth, Germany.

* for correspondence: andreas.moeglich@uni-bayreuth.de
‡ ORCID identifiers: S.S.M.M. 0009-0002-6028-5223; M.H. 0009-0008-2301-3783; C.B. 0000-0002-3552-2349; E.L.R.D. 0009-0000-4156-5428; H.T. 0000-0003-2518-8583; R.U. 0000-0003-2357-1589; A.M. 0000-0002-7382-2772

Abstract

Spatially and temporally orchestrated gene expression underpins organismal development, physiology, and adaptation. In bacteria, two-component systems (TCS) translate environmental cues into inducible expression outputs. Inducible expression also serves as a versatile instrument in both basic and applied science. Here, we harness the photosensors of rhizobial bathy-phytochromes to construct synthetic TCSs for stringent activation of gene expression by near-infrared (NIR) light in laboratory and probiotic *Escherichia coli* strains, and in *Agrobacterium tumefaciens*. Orthogonal TCSs afford the multiplexed expression control of several genes by NIR and visible light. Notwithstanding substantial photochemical activation of bathy-phytochromes by visible radiation, the NIR-light-responsive systems hardly responded to red light. Evidently, light signals can be processed by TCSs into highly nonlinear responses at the physiological relevant level of gene expression. These fundamental aspects likely extend to naturally occurring TCSs. Depending on their photosensor traits

28 and environmental conditions, bathy-phytochromes may thus either be NIR-specific or function as
29 colorblind receptors of light vs. darkness.

30 **Keywords**

31 bacterial phytochrome; gene expression; near-infrared light; optogenetics; sensor histidine kinase;
32 sensory photoreceptor; two-component system

33 Introduction

34 Proportionate to its essential roles in organismal physiology, development, replication, and
35 adaptation, gene expression is stringently and precisely regulated. Various cellular circuits integrate
36 cognate input signals and, in turn, ramp up or down the expression of target genes. Molecular
37 analyses of these circuits not only benefit fundamental research, but also, they underlie applications
38 in biotechnology and synthetic biology for the precise control of gene expression. Two-component
39 systems (TCS) are the predominant signal-transduction pathways by which bacteria and several
40 other organisms process environmental stimuli and convert them into intracellular gene-expression
41 responses (Buschiazzo and Trajtenberg, 2019; Parkinson and Kofoid, 1992). In their canonical form,
42 TCSs comprise as one component a membrane-spanning, homodimeric sensor histidine kinase (SHK)
43 that relays signals to the cell interior. SHKs generally consist of N-terminal extracellular/periplasmic
44 sensor and C-terminal cytosolic effector modules, the latter of which subdivide into the DHp
45 (dimerization and phospho-accepting histidine) and CA (catalytic) domains. In signal-dependent
46 manner, SHKs undergo autophosphorylation at a conserved, eponymous histidine residue to enable
47 subsequent phosphoryl-group transfer to an aspartic acid residue within the response regulator
48 (RR), i.e., the second TCS component. Once phosphorylated, the RR commonly dimerizes and is
49 thereby rendered capable of sequence-specific DNA binding and transcription initiation at target
50 promoters (Gao et al., 2019). As it is the overall levels of phosphorylated RR that govern the

51 physiological output of the TCS, many SHKs are bifunctional and also exert phosphatase in addition
52 to their kinase activities (Möglich et al., 2009; Russo and Silhavy, 1993). Exceedingly stringent and
53 steep regulatory responses can be achieved by finely balancing the opposing RR phosphorylation
54 and dephosphorylation reactions. Depending on the signal, one or the other of the two elementary
55 activities prevails, and the SHK consequently acts as either net kinase or net phosphatase. SHKs are
56 specific for their respective RRs, thus allowing the coexistence in a single cell of multiple TCSs with
57 minimal crosstalk (Laub and Goulian, 2007).

58 Among the plethora of known TCSs, certain representatives respond to light as their cognate
59 stimulus (Möglich, 2019; Ohlendorf and Möglich, 2022). Pertinent TCSs comprise soluble
60 photoreceptor SHKs that reside in the cytosol and absorb light at specific wavelengths within the
61 near-ultraviolet (UV) to near-infrared (NIR) range of the electromagnetic spectrum (Krell et al., 2010;
62 Möglich, 2019). Beyond their pivotal physiological role, these TCSs are of prime interest in
63 biotechnology as they unlock the control of gene expression by light, an approach belonging to
64 optogenetics (Deisseroth et al., 2006). As an inducer of gene expression, light brings several benefits
65 in that it affords superior spatial and temporal precision; can be applied, dosed, and withdrawn with
66 ease and in automatable fashion; and penetrates living tissue to a wavelength-dependent extent
67 (Weissleder, 2001). Several light-responsive TCSs have become available and support strong
68 regulatory responses covering the electromagnetic spectrum from the near-UV to the NIR (Lazar and
69 Tabor, 2021; Ohlendorf and Möglich, 2022). Apart from little-modified naturally occurring setups
70 (Tabor et al., 2011), additional photoreceptor SHKs have been engineered by modular recombination
71 of sensor and effector entities (Levskaya et al., 2005; Möglich et al., 2010, 2009). As a case in point,
72 the widely deployed pDusk and pDawn plasmids resort to the blue-light-inhibited SHK YF1
73 originating from the fusion of a light-oxygen-voltage (LOV) photosensor to the DHp/CA effector of
74 the *Bradyrhizobium japonicum* FixL SHK (Möglich et al., 2009; Ohlendorf et al., 2012). Irrespective

75 of the wealth of setups for the optical control of bacterial gene expression, there is a dearth of
76 circuits affording stringent responses to NIR light (Ong et al., 2018).

77 We previously expanded the pDusk plasmid family by exchanging said LOV photosensor for
78 photosensory core modules (PCM) of bacterial phytochromes (BphP) (Meier et al., 2024a;
79 Multamäki et al., 2022). The resultant pREDusk systems respond to red rather than blue light which
80 facilitates multiplexing (Meier et al., 2024b; Multamäki et al., 2022) with scores of bacterial
81 optogenetic circuits that mostly sense blue light (Ohlendorf and Möglich, 2022). As an added benefit,
82 red light penetrates mammalian tissue to a higher extent than blue light owing to reduced scattering
83 and absorption by cellular constituents, hemoglobin, and other pigments (Ash et al., 2017;
84 Weissleder, 2001). BphPs react to red and NIR light via biliverdin (BV) chromophores covalently
85 attached within their PCMs (Davis et al., 1999; Hughes et al., 1997; Takala et al., 2020). The linear
86 tetrapyrrole BV traverses between the *Z* and *E* isomers of its C15=C16 double bond which underpin
87 the red-absorbing Pr and the far-red-absorbing Pfr states of BphPs, respectively. Red and NIR light
88 triggers the photochromic *Z*/*E* isomerization of BV and thereby drives the photoconversion in the
89 Pr→Pfr and Pfr→Pr directions, respectively. In conventional BphPs, as in those underpinning the
90 pREDusk systems, the Pr state is the thermodynamically more stable form prevailing in darkness.
91 After red-light exposure, these BphPs revert to their Pr resting state thermally within the dark-
92 recovery reaction which is generally protracted and plays out over many hours to days. Conventional
93 BphPs therefore effectively act as ratiometric red/NIR-light sensors. In common with many natural
94 BphP-SHKs (Huber et al., 2024; Karniol and Vierstra, 2003; Lamparter et al., 2002; Multamäki et al.,
95 2021), the engineered ones in the pREDusk circuits exhibit net kinase activity towards their RR within
96 their Pr states and net phosphatase activity within their Pfr states. In pREDusk, red light therefore
97 downregulates target gene expression by several hundred-fold (Meier et al., 2024a; Multamäki et
98 al., 2022). More recently, we inverted the light response of the underlying BphP-SHKs by changing
99 the composition of the linkers through which their sensor and catalytic modules transduce signals

100 (Meier et al., 2024a). Doing so yielded BphP-SHKs with net kinase activity in their Pfr states and net
101 phosphatase activity in their Pr states, thus supporting pronounced increases of gene expression
102 under red light in the resultant pDERusk systems.

103 A second group of bacterial phytochromes, denoted bathy-BphPs, adopt the Pfr rather than
104 the Pr state in darkness (Karniol and Vierstra, 2003). Consequently, NIR light promotes the Pfr→Pr
105 conversion, as does visible light, if to a lesser degree. To the extent it has been studied, the thermal
106 dark recovery in bathy-BphPs is generally fast and complete within seconds to minutes. Due to these
107 aspects, bathy-BphPs are considered to primarily serve as sensors of light vs. darkness rather than
108 of a specific light color (Huber et al., 2024).

109 Informed by spectroscopic analyses, we here harness the PCMs of select bathy-BphPs for
110 stringently controlling TCS output and bacterial gene expression by NIR light. The resultant plasmid
111 systems, dubbed pNIRusk, prompt stringent upregulation of gene expression under NIR light. Equally
112 advantageously and unexpectedly, the engineered pNIRusk circuits show only minimal activation by
113 red light. To enable multiplexed applications, we also advance light-regulated setups based on
114 orthogonal TCSs. The pNIRusk plasmids not only afford pronounced NIR-light responses in
115 *Escherichia coli* laboratory strains but also in the probiotic Nissle bacteria and in *Agrobacterium*
116 *tumefaciens*. Taken together, we deliver versatile implements for the precision control of gene
117 expression by NIR light in both fundamental and applied research.

118 Results

119 Bathy-Bacteriophytochromes as Sensors of Light and pH

120 To subject bacterial gene expression to NIR light, we considered the PCMs of previously reported
121 bathy-BphPs as input modules (Rottwinkel et al., 2010; Tasler et al., 2005). To better inform our
122 choice, we expressed, purified, and spectroscopically characterized BphP PCMs from *Azorhizobium*

123 *caulinodans* (*Ac*PCM), *Agrobacterium vitis* (*Av*PCM), and *Pseudomonas aeruginosa* (*Pa*PCM).
124 Consistent with earlier reports, all three PCMs fully populated the Pfr state in darkness with distinct
125 Soret- and Q-band absorbance peaks at 415 nm and (755 ± 3) nm, respectively (Fig. 1a-c). Exposure
126 to NIR light drove the complete conversion to the Pr state characterized by maxima of the Soret band
127 at (393 ± 2) nm and of the Q band at around (698 ± 3) nm. Illumination with blue and red light
128 prompted partial population of the Pr state to around 65-80% and 40-70%, respectively. Strikingly,
129 at pH 8.0, the Q-band intensity of the pure Pr state differed markedly across the PCMs, with *Pa*PCM
130 showing the strongest signal, and *Ac*PCM the weakest. Based on earlier reports, these data may
131 principally reflect differences in BV protonation at the pyrrole C ring (Borucki et al., 2005; Zienicke
132 et al., 2013). To put this notion to the test, we recorded absorbance spectra for the three PCMs at
133 pH values between 6 and 11 (Fig. 1d-f). While the Q-band intensity remained invariant within the
134 Pfr state, in the Pr state it increased with decreasing pH. By evaluating the corresponding absorbance
135 peak heights as a function of pH, we determined apparent pK_a values of 7.2 ± 0.1, 8.0 ± 0.1, and 9.9
136 ± 0.2 for *Ac*PCM, *Av*PCM, and *Pa*PCM, respectively (Fig. 1g). Following previous studies (Zienicke et
137 al., 2013), we tentatively ascribe these pK_a values to (de-)protonation of the nitrogen atom within
138 the pyrrole C ring in BV. In addition, pH also affects the photostationary Pr:Pfr ratio under red light
139 which increases with rising alkalinity (Fig. 1h, Suppl. Fig. 1a-c).

140 Having ascertained the bathy-character of the candidate PCMs and their Pr⇄Pfr
141 interconversion, we next assessed the kinetics of reversion to their dark-adapted Pfr state at pH 8.0
142 following NIR illumination (Fig. 1i). All three PCMs fully recovered to the Pfr state in single-
143 exponential fashion, but the time constants τ for *Ac*PCM and *Av*PCM of (140 ± 1) s and (80 ± 1) s
144 were markedly lower than the value of (610 ± 1) s for *Pa*PCM. Closely similar recovery time constants
145 resulted after exposing the samples to red instead of NIR light (Suppl. Fig. 1d-e). With rising alkalinity,
146 we observed slower and less complete recovery after NIR-light exposure (Suppl. Fig. 1g-l).

147 Potentially, this deceleration directly owes to BV deprotonation evidenced in the absorbance
148 spectra. That is because BV remains protonated in the Pfr state across all investigated pH values, but
149 within the Pr state it is progressively deprotonated at higher pH values. The return to the Pfr state
150 hence requires re-protonation at elevated pH values which may slow down the dark recovery.

151 **Subjecting Bacterial Gene Expression to NIR-Light Control**

152 To achieve control of bacterial expression by NIR light, we adapted the previous *Dm*REDusk plasmid
153 which encodes a red-light-responsive chimeric SHK originating from the fusion of the PCM of
154 *Deinococcus maricopensis* BphP (*Dm*BphP) to the DHp/CA fragment of *B. japonicum* FixL (Meier et
155 al., 2024a). As seen not least in the above spectroscopic experiments, bathy-BphPs also respond to
156 visible besides NIR light, which stands to cause undesired crosstalk with genetic circuits that react
157 to, e.g., blue or red light. We reasoned that this adverse effect may be ameliorated by deliberately
158 rendering the NIR-responsive systems comparatively insensitive to light. Guided by the above
159 spectroscopic analyses, we selected *Ac*PCM and *Av*PCM as they exhibit a faster Pr→Pfr dark recovery
160 than *Pa*PCM, which translates into a lower effective light sensitivity at photostationary state
161 (Ohlendorf and Möglich, 2022; Ziegler and Möglich, 2015).

162 With *Ds*Red as a fluorescence reporter gene, we replaced *Dm*PCM within *Dm*REDusk by
163 either *Ac*PCM or *Av*PCM, while maintaining the same register for the linker between the PCM and
164 DHp/CA moieties (Suppl. Fig. 2). In the resultant plasmids, referred to as pNIRusk, the heme
165 oxygenase enzyme for intracellular BV provision, the BphP-SHK, and the matching RR FixJ thus form
166 a constitutively expressed tricistronic operon (Fig. 2a). The initial pNIRusk designs, denoted '0',
167 showed considerable reporter fluorescence in darkness that only slightly elevated under both red
168 and NIR light, despite their BphP-SHKs adhering to the same design as in *Dm*REDusk (Fig. 2b).

169 Spurred by our recent construction of the pDERusk setups (Meier et al., 2024a), we
170 hypothesized that light responsiveness may be installed by varying the composition of the linker
171 between the PCM and DHp/CA moieties. That is because this linker is expected to adopt continuous
172 α-helical coiled-coil conformation and serves as the conduit for conformational signals traveling from
173 the PCM to the effector module (Diensthuber et al., 2013). Using the PATCHY approach (Ohlendorf
174 et al., 2016), we generated libraries of the *Ac*NIRusk and *Av*NIRusk setups that differ in the length
175 and sequence of said linker. In brief, the PATCHY protocol achieves linker variation by randomly
176 recombining different portions of the linkers deriving from the parental receptors, i.e., the bathy-
177 BphP PCM and the FixL SHK, respectively (see Suppl. Fig. 3). By assessing the reporter fluorescence
178 in darkness and under NIR and red light, we identified five light-switchable variants for *Ac*NIRusk and
179 six for *Av*NIRusk (Fig. 2b, Suppl. Fig. 3). Variants were considered light-switchable if they exhibited at
180 least a 2-fold difference in reporter fluorescence in darkness vs. illumination with either red or NIR
181 light. We refer to individual variants by their linker lengths relative to the initial constructs. Although
182 the light-responsive variants all rely on the same PCMs and DHp/CA modules, they drastically
183 differed in their response to NIR light, with some elevating and others lowering reporter-gene
184 expression compared to darkness. Earlier application of PATCHY to SHKs responding to blue and red
185 light (Meier et al., 2024a; Ohlendorf et al., 2016) had pinpointed sets of light-regulated receptor
186 variants that exhibited systematic trends in the distribution of the underlying linkers. Specifically,
187 receptor variants differing in their linker length by multiples of seven residues tended to show similar
188 responses to light, which could be rationalized by the coiled-coil nature of said linkers (Diensthuber
189 et al., 2013; Ohlendorf et al., 2016). At present, we only identified a handful of light-responsive SHK
190 variants, thus largely precluding systematic analyses of the linker properties.

191 We subsequently focused on variants inducing gene expression under NIR light, albeit with
192 intriguing variation in their response to red light. For instance, *Ac*NIRusk-1b with a linker one residue

193 shorter than in *Dm*REDusk showed sizeable induction under red light. By contrast, the variant
194 *Ac*NIRusk-1a with the same linker length but different sequence did much less so. For an eventual
195 application, we deem a reduction of red-light-induced activation advantageous. We thus continued
196 with *Ac*NIRusk-1a and *Av*NIRusk+17a, both of which strongly induce expression under NIR light
197 compared to darkness but only show small responses to red light. For simplicity, we refer to these
198 setups as *Ac*NIRusk and *Av*NIRusk in the following.

199 Flow cytometry revealed homogeneous single-cell fluorescence distributions for *E. coli*
200 bacteria harboring *Ac*NIRusk or *Av*NIRusk (Fig. 2c). When incubated in darkness, the median
201 fluorescence was only 2-fold above the background fluorescence. Saturating NIR light (800 nm, 250
202 µW cm^{-2}) induced largely uniform shifts of the entire cell population to several 10-fold higher median
203 fluorescence for *Ac*NIRusk and *Av*NIRusk, respectively, an effect similar in magnitude to the red-light
204 response observed previously for the pDERusk systems (Meier et al., 2024a). At sub-saturating light
205 doses, the single-cell fluorescence of bacteria containing *Ac*NIRusk and *Av*NIRusk uniformly rose to
206 intermediate levels with increasing NIR-light intensity (Suppl. Figs. 4 and 5a-b). Red (100 µW cm^{-2})
207 and blue (70 µW cm^{-2}) light partially activated *Ac*NIRusk 11-fold and 35-fold, respectively (Fig. 2c).

208 At the ensemble level, the average fluorescence per cell density ramped up sigmoidally with
209 NIR light by up to around 70- and 150-fold for *Ac*NIRusk and *Av*NIRusk, respectively (Fig. 2d-e). The
210 two systems exhibited half-maximal activation at relatively high NIR-light intensities of (29 ± 1) µW
211 cm^{-2} and (43 ± 1) µW cm^{-2}, i.e., about an order of magnitude above the half-maximal red-light doses
212 previously determined for induction of the pREDusk and pDERusk systems (Meier et al., 2024a;
213 Multamäki et al., 2022). Arguably, these differences reflect at least in part the respective dark-
214 recovery times of the underlying bathy-BphPs which are in the seconds to minutes range rather than
215 in the hours range for conventional BphPs. Bacterial cell growth was unaffected by NIR light (Suppl.
216 Fig. 5c-e).

217 Red light also induced *Ac*NIRusk and *Av*NIRusk but only around 2- and 6-fold relative to
218 darkness (Fig. 2d-e). Blue light elicited a stronger 16- and 25-fold induction, respectively, at the
219 highest probed light intensity of around 120 µW cm^{-2}. Higher blue-light intensities were not accessed
220 owing to instrumental limitations and onsetting phototoxicity. From the data, we determined half-
221 maximal blue-light doses of (46 ± 3) µW cm^{-2} and (100 ± 20) µW cm^{-2} for *Ac*NIRusk and *Av*NIRusk,
222 respectively. Given the around 1.7-fold higher energy of blue compared to NIR light, the circuits
223 therefore trigger at similar half-maximal photon fluencies for either light color. At least qualitatively,
224 the degree of induction by the individual light colors (red, blue, NIR) follows the same trend as the
225 photochemical responses evidenced in the underlying *Ac*PCM and *Av*PCM (see Fig. 1a-c) where NIR
226 light elicited the most pronounced Pr formation, followed by blue and red light.

227 **Engineering Orthogonal Light-responsive Two-Component Systems**

228 In common with earlier members of the pDusk pedigree, the pNIRusk systems are based on the FixLJ
229 TCS from *B. japonicum* (Anthamatten and Hennecke, 1991). Combinations of several of these setups
230 would hence experience crosstalk at the level of RR phosphorylation which, in all but a few cases, is
231 undesired. To overcome this limitation, we set out to engineer light-responsive TCSs orthogonal to
232 those used in pDusk, pNIRusk, and related setups. As recently surveyed, several TCSs have been
233 characterized to the point that they have found application in synthetic biology (Lazar and Tabor,
234 2021). Based on their reported stringency of regulation, we selected as candidate TCSs TtrSR from
235 *Shewanella baltica* that responds to tetrathionate and TodST from *Pseudomonas putida* that can
236 detect toluene compounds (Daeffler et al., 2017; Lau et al., 1997).

237 Starting from *Dm*REDusk, we substituted the original FixL DHp/CA domains for those from
238 TtrS, while also exchanging FixJ for the TtrR RR and putting the expression of a *Ds*Red reporter under
239 control of the Pttr promoter that is subject to regulation by TtrSR (Fig. 3a). Within this framework,
240 we then varied the linker interconnecting the *Dm*PCM and the TtrS DHp/CA module via PATCHY

241 (Ohlendorf et al., 2016). Screening of the resultant linker library for differential *Ds*Red expression
242 under darkness, and NIR and red light identified several variants, termed *Dm*Ttr, with substantial
243 light responses (Fig. 3a, Suppl. Fig. 6a). Notably, the overall expression levels within the identified
244 *Dm*Ttr systems were markedly higher than those in the pREDusk and pNIRusk setups.

245 Next, we extended the strategy to *Av*NIRusk by introducing TodST. Of note, TodS is a complex
246 SHK with integrated phosphorelay that comprises in sequential order PAS-1, DHp-1, CA-1, REC, PAS-
247 2, DHp-2, and CA-2 domains (Busch et al., 2009). Toluene signals, detected by PAS-1, modulate the
248 activity of the DHp-1/CA-1 unit which phosphorylates the REC domain that in turn governs the
249 activity of the DHp-2/CA-2 module and eventual phosphorylation of the TodT RR. Earlier reports
250 showed that a miniaturized TodS variant only comprising the PAS-1, DHp-2, and CA-2 domains,
251 dubbed Min-TodS, retains toluene sensitivity and stringent regulation of TodT (Silva-Jiménez et al.,
252 2012). Consequently, we replaced the FixLJ TCS in *Av*NIRusk by the TodS DHp-2/CA-2 fragment, while
253 also introducing the TodT RR and its cognate PtodX promoter (Fig. 3b). Linker variation by PATCHY
254 and screening for *Ds*Red reporter fluorescence pinpointed several variants, termed *Av*Tod, which
255 either elevated or lowered gene expression in response to NIR light (Fig. 3b, Suppl. Fig. 6b).

256 For further analyses, we selected the variants *Dm*Ttr+7b, *Av*Tod+16, and *Av*Tod+21 with PCM-
257 DHp/CA linkers 7, 16, and 21 residues, respectively, longer than that in the parental *Dm*REDusk
258 circuit. Exposed to red light, *Dm*Ttr+7b elicited an about 15-fold decrease of gene expression
259 compared to darkness (Suppl. Fig. 7a). Whereas *Av*Tod+16 supported a 20-fold reporter-
260 fluorescence decrease under NIR light, *Av*Tod+21 promoted an 8-fold increase of gene expression
261 (Suppl. Fig. 7b-c). Although the attained regulatory efficiencies pale in comparison to those of
262 *Dm*REDusk (Meier et al., 2024a) and *Av*NIRusk, the data show that the principal design and screening
263 strategies readily translate to other TCSs.

264 To allow multiplexing of several light-responsive circuits in a single bacterial cell, we modified
265 the *Dm*DERusk and *Av*NIRusk plasmids by replacing their kanamycin resistance marker, their ColE1

266 origin of replication (ori), and their *Ds*Red reporter gene by a streptomycin marker, the CloDF13 ori,
267 and the yellow-fluorescent YPet reporter, respectively. The resultant *Dm*DERusk-Str-YPet and
268 *Av*NIRusk-Str-YPet circuits showed similar responses to red and NIR light as the parental plasmids
269 they derive from (Suppl. Fig. 7d-e). Pairs of compatible plasmids with different TCSs, oris, resistance
270 markers, and fluorescent reporters were transformed into bacteria, followed by cultivation in
271 darkness, under red (100 µW cm^{-2}) or NIR light (200 µW cm^{-2}), or under both light colors. By
272 employing individual plasmid combinations, the expression of the *Ds*Red and YPet reporters could
273 be individually controlled by the two light colors (Fig. 3c, Suppl. Fig. 7f). For instance, when
274 combining *Dm*DERusk-Str-YPet with *Av*Tod+21-*Ds*Red, YPet and *Ds*Red expression rose under red and
275 NIR light, respectively, whereas the joint application of both light colors only induced the YPet
276 reporter gene. Taken together, well-chosen plasmid sets enable the orthogonal expression control
277 of two target genes by red and NIR light. Notably, the plasmids can be deployed as is with no further
278 modifications required.

279 Although not probed here, the overall performance and relative response in multiplexed
280 applications may be optimized by variation of the copy number and expression strength of the
281 individual plasmids. Likewise, rather than using saturating light intensities as in the above
282 experiments, yet finer-grained expression control could be exerted by adjusting the red- and NIR-
283 light intensities. In a similar vein, different wavelengths, currently determined by the available
284 instrumental setups, may be chosen to better separate the individual light responses of two (or,
285 several) multiplexed systems.

286 **Applications in the Laboratory and Beyond**

287 As TCSs widely recur across bacterial phyla, they often retain functionality upon transfer between
288 different bacterial strains. Earlier reports not least demonstrated that representatives of the pDusk
289 family support light-regulated gene expression across several prokaryotes (Ohlendorf and Möglich,

290 2022). For instance, pDusk and its derivative pDawn (Ohlendorf et al., 2012) have been successfully
291 deployed in *E. coli* Nissle 1917 (*Ec*N) and other probiotic bacteria (Cui et al., 2021; Magaraci et al.,
292 2014; Pan et al., 2021; Sankaran and del Campo, 2019; Yang et al., 2020). These experiments augur
293 the application of light-responsive bacteria in the gut of mammals as programmable, living
294 therapeutics (Ohlendorf and Möglich, 2022). To date, however, pertinent applications are limited by
295 the shallow tissue penetration of blue light required for triggering pDusk and pDawn. Although
296 upconverting nanoparticles can be administered jointly with the light-responsive bacteria to allow
297 actuation by NIR light, this approach introduces complexity and departs from a fully self-contained,
298 optogenetic strategy (Yang et al., 2020). To assess whether the presently generated light-responsive
299 gene-expression systems may overcome this potential limitation, we introduced *Ac*NIRusk and
300 *Av*NIRusk into *Ec*N. Both setups mediated a more than 100-fold upregulation of reporter-gene
301 expression under NIR light with half-maximal doses of (27 ± 1) and (28 ± 2) µW cm^{-2}, respectively
302 (Fig. 4a, Suppl. Fig. 8). Of advantage, the response to blue and NIR light was even lower than
303 observed above for the *E. coli* laboratory strain.

304 We next probed the performance of *Av*NIRusk and *Dm*REDusk in the biotechnologically
305 relevant *Agrobacterium tumefaciens*. To this end, we constructed derivative plasmids, denoted
306 *Av*NIRlux and *Dm*REDlux, that subject the expression of a luciferase operon under the control of the
307 light-responsive TCSs (Fig. 4b). After conjugational transfection into *A. tumefaciens*, the light
308 response was assessed by spotting the bacteria on agar plates (Fig. 4c). As visualized by
309 luminescence, the *Av*NIRlux system strongly induced expression upon incubation under NIR light
310 compared to darkness. Different from *E. coli* (see Fig. 2e, Suppl. Fig. 9a), red light activated to similar
311 extents as NIR light, whereas blue light induced expression only weakly. In the case of *Dm*REDlux,
312 the expression of the *lux* reporter was strongly reduced under both blue and red light, but not under
313 NIR light or in darkness. Although *A. tumefaciens* harbors two endogenous BphPs (Karniol and
314 Vierstra, 2003), our experiments did not detect any differences in growth or phenotype between

315 cultivation under NIR and red light. We next characterized the response of *A. tumefaciens* cultured
316 in liquid medium. Once reaching the stationary phase after around 20 h (Suppl. Fig. 9b), the cultures
317 bearing *Av*NIRlux exhibited a 7-fold activation of *lux* expression by NIR light compared to darkness.
318 For *Dm*REDlux, the *lux* expression was around 300-fold higher in darkness than under red light (Fig.
319 4d, Suppl. Fig. 9c-d).

320 **Discussion**

321 **Bathy-Bacteriophytochromes as Tunable Sensors of Light Intensity and Quality**

322 As conventional bacteriophytochromes do, bathy-BphPs transition between their Pr and Pfr states
323 with 15*Z*- and 15*E*-configured biliverdin, respectively. In marked contrast to the conventional
324 representatives, bathy-BphPs assume their 15*E*-configured Pfr state as the thermodynamically most
325 stable form in darkness, rather than their Pr state. Despite this principal difference, the overall PCM
326 architecture and the residues lining the bilin binding pocket are remarkably conserved across known
327 BphPs. Notwithstanding limited successes in reprogramming certain BphPs (Böhm et al., 2025; Xu et
328 al., 2024), the molecular determinants underlying bathy-character remain elusive and their design
329 demanding.

330 Owing to their Pfr dark-adapted state, bathy-BphPs undergo net Pfr→Pr conversion when
331 irradiated with light within the near-UV to NIR region of the electromagnetic spectrum. Put another
332 way, there is no light quality that would fully populate the dark-adapted Pfr state. Bathy-BphPs
333 surmount this challenge by a fast thermal Pr→Pfr recovery that restores the Pfr state within seconds
334 to minutes. The primary physiological role of bathy-BphPs may hence be that of sensors of light
335 quantity rather than quality (i.e., color) (Huber et al., 2024).

336 Intriguingly, we uncovered a profound pH influence on photoreception in bathy-BphPs. With
337 rising alkalinity, the absorption cross-section of the Q band strongly decreases within the Pr state

338 but remains unchanged for Pfr. Based on earlier studies (Borucki et al., 2005; Velazquez Escobar et
339 al., 2015; Zienicke et al., 2013), we attribute these spectral changes to (de-)protonation of the
340 nitrogen atom of the BV pyrrole C within the Pr state. The pertinent pK_a values range between 7-8
341 for *Ac*PCM and *Av*PCM, similar to the value of 7.6 for the bathy-BphP Agp2 from *A. tumefaciens*
342 (Zienicke et al., 2013), but substantially lower than the value of about 10 for *Pa*PCM. Inspection of
343 the experimentally determined *Pa*PCM and Agp2PCM structures in their Pfr states (Schmidt et al.,
344 2018; Yang et al., 2008) and the corresponding Pfr models for *Ac*PCM and *Av*PCM (Abramson et al.,
345 2024) reveals highly conserved chromophore-binding pockets with most residues adjacent to BV
346 identical in all four proteins (Suppl. Fig. 10). However, *Pa*PCM features tyrosine and serine residues
347 at positions 190 and 275 rather than phenylalanine and alanine, respectively, in the equivalent
348 places of the other three PCMs. Although speculative at present, these systematic differences may
349 render the *Pa*PCM binding pocket comparatively hydrophilic and thereby account for the divergent
350 protonation equilibrium of the pyrrole C ring.

351 BV deprotonation within the Pr state at elevated pH incurs at least three principal effects that
352 under constant light all promote population of the Pr state at the cost of the Pfr state. First, the
353 Pr→Pfr dark recovery slows down between pH 7 and 10 for all three investigated PCMs. At least in
354 part, this may reflect the need for BV re-protonation upon return from the Pr to the Pfr state which
355 remains fully protonated at all investigated pH values. Second, as noted above, BV deprotonation
356 leads to a drastic reduction of the Q-band absorbance within the Pr state (see Fig. 1). For a given
357 intensity of visible light, photoconversion to the Pfr state thus becomes less effective, thereby again
358 favoring the Pr state at photostationary state. Third, BV deprotonation also goes along with a
359 dramatic decrease in the apparent photoconversion quantum yields in the Pr→Pfr vs. the Pfr→Pr
360 directions (Suppl. Fig. 1f). As best exemplified for *Ac*PCM, at pH 6.5, the respective quantum yields
361 for the photoreversible Pr⇄Pfr interconversion are about equal, but at pH 10.5, the quantum yield
362 in the Pr→Pfr direction is less than 1% that in the Pfr→Pr direction. Together with the pH-dependent

363 reduction in the Pr-state Q-band absorbance, this mechanism leads to vastly different red-light-
364 induced photostationary states as a function of pH (see Fig. 1h). Whereas at low pH, saturating red
365 light results in about 60-70% Pfr population, at high pH values almost no Pfr state remains (Fig. 5).
366 As a direct consequence, at pH 10.5, red light counter-intuitively drives the complete conversion to
367 the Pr state of *Ac*PCM. Put another way, in its deprotonated form this bathy-BphP becomes
368 essentially colorblind and acts as a pure light-intensity sensor. Although less pronounced, *Av*PCM
369 and *Pa*PCM follow the same trend with pH.

370 While it is debatable whether the rhizobia *Ac*PCM and *Av*PCM derive from ever encounter
371 such extreme pH swings, it has been proposed that the resultant changes in photochemical
372 properties could serve a sensing function (Zienicke et al., 2013). Even independent of this aspect,
373 our present analyses show how pH impacts bathy-BphP photoreception at multiple levels. While it
374 remains true that all light colors net promote the Pfr→Pr transition, they do so to different extents
375 which can have a profound impact on downstream signal transduction as discussed below. We
376 propose that modulation of the BV protonation midpoint has been harnessed during evolution to
377 sculpt the light response of extant bathy-BphPs according to the individual needs of the respective
378 organism of origin. In line with this hypothesis, we presently evidence a considerable span of pK_a
379 values for BV protonation across several bathy-BphP PCMs.

380 **Engineering of NIR-Light-Responsive Proteins**

381 As best exemplified by sensor histidine kinases, PCMs of bathy-BphPs can occur in conjunction with
382 the same type of effector as those of conventional BphPs (Blum et al., 2025). However, it has been
383 unclear whether a single, specific output protein can be regulated in its activity by both PCM types.
384 The successful recombination of bathy-BphP PCMs with the same DHp/CA module earlier controlled
385 by conventional BphP PCMs (Meier et al., 2024a; Multamäki et al., 2022) now demonstrates the
386 principal validity of this idea. At least to some extent, the PCMs of conventional and bathy-BphPs are

387 hence interchangeable, a finding that indicates shared or compatible signal-transduction
388 mechanisms, as also suggested by the conserved structure and photochemistry across the BphP
389 class (Möglich, 2019; Takala et al., 2020). As one important ramification, numerous previously
390 engineered red-light-responsive receptors may thus be subjugated to NIR-light control by swapping
391 out their underlying PCMs from conventional BphPs for ones from bathy-BphPs (Chernov et al.,
392 2017; Etzl et al., 2018; Leopold et al., 2022, 2019; Levskaya et al., 2005; Schmidl et al., 2014; Stabel
393 et al., 2019; Stüven et al., 2019; Tang et al., 2021). Compared to the challenging approach of
394 imparting bathy-character via limited PCM modifications (Böhm et al., 2025; Xu et al., 2024), the
395 design task thus considerably simplifies.

396 We identify several caveats that likely hold for future design endeavors, too. Notably, the
397 connection between PCM and effector of choice needs to be conducive to transmitting light signals.
398 When at present employing the same linker register that supports red-light-inhibited gene
399 expression in *Dm*REDusk, we initially derived *Ac*PCM- and *Av*PCM-based systems giving rise to
400 constitutive target gene expression without pronounced light responses. Adjusting the length and
401 sequence of the linker intervening the PCM and the DHp/CA domains then yielded variants with
402 robust gene-expression responses to NIR light. Based on structural and biochemical evidence, said
403 linker is expected to form a continuous parallel α-helical coiled coil within the homodimeric SHK
404 (Bódizs et al., 2024; Burgie et al., 2024; Diensthuber et al., 2013; Jacob-Dubuisson et al., 2018; Malla
405 et al., 2024; Möglich, 2019; Möglich et al., 2009). Although other BphP-based photoreceptor designs
406 may involve linkers adopting different structures, the variation and probing of length and sequence
407 variants generally represents a worthwhile strategy that may eventually bear fruit. As, depending on
408 the use case, sizeable variant libraries may have to be assessed, two principal aspects emerge that
409 benefit the implementation of this strategy. First, the construction of libraries covering the desired
410 diversity in linker composition should be efficient, which can, e.g., be achieved by resorting to the
411 PATCHY protocol (Ohlendorf et al., 2016) as done here. Second, the screening for light-regulated

412 function should afford sufficient throughput, e.g., by coupling photoreceptor function to a
413 fluorescent readout or cell survival.

414 **Tunability of NIR-Light-Activated Two-Component Systems**

415 The recombination of bathy-BphP PCMs with a SHK effector module led to the pNIRusk plasmids for
416 stringent activation by NIR light of bacterial gene expression. As the underlying PCMs absorb light
417 over the entire near-UV to NIR region of the electromagnetic spectrum, the pNIRusk systems are
418 expected to also activate when exposed to other light colors. To dampen the commonly undesirable
419 activation by visible light and thereby facilitate the multiplexing with other photoresponsive circuits,
420 we deliberately chose *Ac*PCM and *Av*PCM because of their comparatively fast Pr→Pfr thermal
421 recovery. At photostationary state under constant illumination, a faster recovery results in an
422 effective desensitization against light, be it of blue, red, or NIR color (Ziegler and Möglich, 2015).
423 Consistent with this design rationale, the *Ac*NIRusk and *Av*NIRusk setups indeed exhibit half-maximal
424 light doses around ten times higher than for, e.g., *Dm*DERusk which relies on a conventional BphP
425 PCM (Meier et al., 2024a). Given its low phototoxicity, NIR light may be applied at even high powers
426 without harming the biological system under study. We note that NIR light around 800 nm is
427 commonly used in a therapeutic setting for photobiomodulation at intensities exceeding the ones
428 presently used by up to several orders of magnitude (Hamblin, 2016).

429 Perplexingly, the *Ac*NIRusk and *Av*NIRusk circuits respond moderately or very weakly to blue
430 and red light, respectively (see Fig. 2d, e). Although the strength of the gene-expression response
431 monotonically increases with the extent of Pfr→Pr photoconversion elicited by the individual light
432 colors within the underlying PCMs (see Fig. 1a-c), there is no direct proportionality. For instance,
433 *Ac*PCM roughly assumes a 0.7:0.3 photostationary Pr:Pfr equilibrium under red light (see Fig. 1a),
434 but at the level of gene expression, the response of the *Ac*NIRusk circuit to red light is only 2% that
435 of the NIR-light response. Initially unexpected, this baffling effect therefore further benefits the

436 application of the pNIRusk circuits in combination with other light-responsive entities, be it
437 optogenetic circuits or fluorescent reporters (Meier et al., 2024b; Tabor et al., 2011).

438 Our work provides pointers to the potential molecular underpinnings in that we isolated
439 additional pNIRusk variants with similar NIR-light responses but substantially higher expression
440 under red light (see Fig. 2b). Notably, these variants only differ in the composition of their linkers
441 connecting PCM to effector. Informed by our recent investigation of linker variants that culminated
442 in the generation of *Dm*DERusk (Meier et al., 2024a), we hypothesize that the different red-light
443 responses find their origin in an altered balance between the counteracting elementary histidine
444 kinase and phosphatase activities of SHKs. At the ensemble level, even small perturbations, e.g.,
445 caused by linker variation or changes in the Pr:Pfr proportion, can utterly tilt the net activity in either
446 the kinase or phosphatase direction (Landry et al., 2018; Möglich, 2019; Möglich et al., 2009; Russo
447 and Silhavy, 1993). The histidine kinase-phosphatase duality of TCSs thus provides a means of
448 rendering the signal response to light highly malleable and adaptable. At a practical level, when
449 engineering light-responsive TCSs, we advise to screen multiple candidate variants that may well
450 differ substantially in their signal response. As noted previously (Meier et al., 2024a), similar
451 concepts may also operate for cyclases (GGDEF) and phosphodiesterases (EAL) enzymes that
452 frequently occur in conjunction with BphP PCMs (Gourinchas et al., 2017) and that antagonistically
453 catalyze the making and breaking, respectively, of the bacterial second messenger cyclic-di-
454 guanosine monophosphate (Jenal et al., 2017).

455 **Applications in the NIR Future**

456 The advent of stringently controlled NIR-responsive bacterial gene-expression platforms now
457 facilitates a number of innovative applications. First, the currently available optogenetic setups for
458 expression regulation in bacteria predominantly respond to blue and red light but are often blind to
459 NIR light (Ohlendorf and Möglich, 2022). Given their fully intended relative insensitivity and their

460 unexpectedly weak response to visible light, the pNIRusk systems lend themselves to combinations
461 with pertinent setups. For example, applied at low to moderate intensity, blue light would trigger
462 one setup, e.g., pAurora2 or EL222-based systems (Jayaraman et al., 2016; Ranzani et al., 2024), but
463 leave pNIRusk largely untouched. By contrast, NIR light would selectively activate pNIRusk as the
464 LOV receptors underlying the blue-light-responsive setups are insensitive to this light quality. To
465 facilitate multiplexed applications of pNIRusk, we supply derivatives reliant on alternative TCSs that
466 can be readily combined in single bacterial cells and mediate the expression of several target genes
467 orchestrated by two light colors.

468 Second, NIR light penetrates mammalian tissue much more deeply than light of shorter
469 wavelengths (Lehtinen et al., 2022; Weissleder, 2001), owing to reduced absorption and scattering
470 which are, e.g., 5-10 lower for near-infrared light than for blue light. The exponential attenuation of
471 light intensity with tissue depth is therefore much less pronounced for NIR light than it is for UV or
472 visible light. Given the low phototoxicity of NIR light and its established use in photobiomodulation,
473 noted above, the pNIRusk setups stand to be activatable through substantial tissue layers of at least
474 several millimeters. Although the pNIRusk setups are (deliberately) less light-sensitive than, e.g., the
475 earlier pREDusk and pDERusk systems, they can be nonetheless actuated by light fluences in the
476 range of several tens of µW per cm^2 which is orders of magnitudes less than the light intensities
477 commonly used in neuronal optogenetics. These aspects open up intriguing applications involving
478 programmable, light-responsive bacteria as agents inside the bodies of mammals, e.g., as living
479 therapeutics (Cubillos-Ruiz et al., 2021; Hartsough et al., 2020). The pDawn system has already been
480 applied in this capacity within probiotic bacteria, but the approach has been hampered by delivering
481 blue light *in situ* (Cui et al., 2021; Magaraci et al., 2014; Pan et al., 2021; Sankaran and del Campo,
482 2019; Yang et al., 2020). One remedy has been the use of upconverting nanoparticles (UCNP)
483 administered alongside the light-responsive bacteria (Pan et al., 2021; Yang et al., 2020). Notably,
484 the UCNPs can be charged by absorption of several photons in the NIR range to then emit a photon

485 in the blue spectral region. Though feasible, pertinent applications introduce complexity and depart
486 from a purely genetically encoded optogenetic strategy. The new pNIRusk setups directly address
487 this challenge as they can be activated by wavelengths closely similar to those previously used for
488 charging the UCNPs but at around 10-fold lower light intensity. Towards this goal, we demonstrate
489 at present that both *Ac*NIRusk and *Av*NIRusk operate in the probiotic *E. coli* Nissle strain out of the
490 box, without need for optimization. Used in place of pDawn, the pNIRusk systems thus obviate the
491 need for the UCNPs and thereby broaden the application scope of living therapeutics considerably.

492 Third, we demonstrate functionality of pNIRusk and pREDusk in the biotechnologically
493 relevant *A. tumefaciens* (Fig. 4c-d) which is widely used as a transfection vehicle in plant
494 biotechnology (Liu et al., 2013). Prospectively, both pNIRusk and pREDusk may achieve
495 spatiotemporal control of *A. tumefaciens* infectivity, e.g., to confine plant transfection to specific
496 time windows or organs. Of particular advantage, the bathochromically shifted absorbance spectra
497 of BphPs compared to plant Phys (Hughes and Winkler, 2024; Yi et al., 2025) stand to enable NIR-
498 light control without interfering with plant photoreception and photoautotrophic growth.

499 **Methods**

500 **Molecular Biology**

501 Oligonucleotides and plasmids used in this study are listed in Suppl. Tables 1 and 2. All plasmid
502 constructs were confirmed by Sanger sequencing (Microsynth Seqlab, Göttingen, Germany). To
503 produce bathy-BphP PCMs, the respective genes were introduced into a pCDF-Duet plasmid
504 (Novagen) already containing heme oxygenase 1 (HO1) from *Synechocystis* sp. for biliverdin supply
505 (Mukougawa et al., 2006; Stüven et al., 2019). To this end, the genes encoding the PCMs from *A.*
506 *caulinodans* (Uniprot A8HU76, residues 1-501), *A. vitis* (Uniprot B9JR96, residues 1-499), and *P.*
507 *aeruginosa* (Uniprot Q9HWR3, residues 1-497) were amplified by PCR from the template plasmids

508 pQX091, pQX086, and pQX037, respectively (Xu et al., 2024), followed by Gibson assembly (Gibson
509 et al., 2009).

510 The initial *Ac*NIRusk and *Av*NIRusk constructs (denoted '0') were created by exchanging
511 *Dm*PCM in *Dm*REDusk (Meier et al., 2024a) for *Ac*PCM and *Av*PCM, respectively (Suppl. Fig. 2), via
512 PCR amplification and Gibson assembly. The second amino acid in *Ac*PCM and *Av*PCM was changed
513 from proline to threonine to maintain the polycistronic structure of the operon comprising HO1, the
514 BphP-SHK, and the RR FixJ. To apply the PATCHY strategy (Ohlendorf et al., 2016), start constructs
515 were generated by elongating the PCM-DHp/CA linkers in the initial *Ac*NIRusk and *Av*NIRusk plasmids
516 as reported before (Meier et al., 2024a). The resulting constructs thus comprise the N-terminal
517 portions of the parental BphPs from A. *caulinodans* (Uniprot A8HU76) and *A. vitis* (Uniprot B9JR96)
518 up to and including residues 520 and 518, respectively, connected to the C-terminal fragment of *B.*
519 *japonicum* FixL starting from residue 257 (Uniprot P23222). At the junction, a restriction site for
520 *Ksp*AI and a one-nucleotide frameshift were inserted (Suppl. Fig. 3). Cloning was performed by two
521 consecutive overhang-PCRs and blunt-end ligation.

522 The TtrSR TCS from *Shewanella baltica* was introduced into *Dm*REDusk (Meier et al., 2024a)
523 by first replacing the FixK2 promoter by the 85-bp minimal promoter sequence PttrB185-269
524 (Daeffler et al., 2017) via PCR amplification and restriction cloning using *Bgl*II and *Xba*I sites. Next,
525 the *B. japonicum* FixLJ TCS was exchanged for the *S. baltica* TtrSR (Genbank CP000891.1, loci
526 Sbal195_3858 and Sbal195_3859) via Gibson assembly using as a PCR template a synthetic gene
527 (Gene Art) with codons optimized for expression in *E. coli*. For conducting PATCHY, a start construct
528 was made that includes residues 1-539 of the *Dm*BphP (Uniprot E8U3T3) and the *S. baltica* TtrSR
529 TCS (Uniprot A9L3S5) starting at residue 407. Cloning was performed as described above except that
530 an *Eco*32I restriction site and a two-nucleotide frameshift were placed at the junction between the
531 two gene fragments (Suppl. Fig. 6a).

532 The cognate TodX promoter of the TodST TCS from *Pseudomonas putida* was amplified by
533 PCR from pMIR77 (Ramos-González et al., 2002) and inserted into pDusk (Ohlendorf et al., 2012) by
534 restriction cloning with *Bgl*II and *Xba*I. Next, the TodST TCS was amplified from pMIR66 (Ramos-
535 González et al., 2002) and fused to the *Bacillus subtilis* YtvA LOV domain within pDusk via Gibson
536 cloning. The *Av*Tod-NIRusk PATCHY start construct was obtained by replacing YtvA-LOV with HO1 and
537 and *Av*PCM (residues 1-518) via Gibson assembly. The resultant construct comprised the TodS
538 starting from residue 726 (Uniprot E0X9C7) and TodT. At the junction, a *KspA*I restriction site and a
539 one-nucleotide frameshift were inserted (Suppl. Fig. 6b).

540 For multiplexing experiments, the *Ds*Red Express2 reporter gene (Strack et al., 2008) in
541 *Dm*DERusk and *Av*NIRusk was replaced by the YPet reporter gene (Nguyen and Daugherty, 2005).
542 Additionally, the kanamycin (Kan) resistance marker and the ColE1 origin of replication (ori) were
543 exchanged for streptomycin (Str) and a CloDF13 ori via Gibson assembly. A version of *Av*NIRusk
544 containing a multiple-cloning site rather than a fluorescent reporter was cloned by Gibson assembly
545 and deposited at Addgene for distribution (accession number 235084).

546 To apply *Dm*REDusk and *Av*NIRusk in *Agrobacterium tumefaciens*, the *Photorhabdus*
547 *luminescence luxABCDE* operon from pBAM2-luxAE (Dziuba et al., 2021) was cloned into the miniTn5
548 delivery plasmid pBAM2 (Uebe, unpublished). The sequence was amplified via PCR, digested with
549 *Nde*I/*Sac*I, and ligated into a similarly digested and Fast-AP-dephosphorylated pBAM2 vector to
550 generate pBAM2-luxAE. Subsequently, the light-regulated TCS cassettes of *Dm*REDusk (*DrhemO-*
551 *Dmpcm-BjfixL*) and *Av*NIRusk (*DrhemO-Avpcm-BjfixL*) were amplified. These genes were set under
552 the control of the strong constitutive *M. gryphiswaldense* PmamDC promoter. The *B. japonicum*
553 FixK2 promoter was also amplified by PCR. The amplified fragments were fused by overlap extension
554 PCR and digested with *Nde*I/*Not*I as was the pBAM2-luxAE. Ligation resulted in the reporter plasmids
555 *Dm*REDlux and *Av*NIRlux in which the *luxABCDE* operon is under the control of the FixK2 promoter.

556 **Protein Purification**

557 For production of *Ac*PCM, *Av*PCM, and *Pa*PCM, *E. coli* LOBSTR cells (Andersen et al., 2013) were
558 transformed with the respective pCDF-Duet-PCM/HO1 constructs. Gene expression and protein
559 purification were performed as before (Meier et al., 2024a). Briefly, two flasks with 800 mL lysogeny
560 broth (LB) medium each supplemented with 100 µg mL^{-1} Str were inoculated with a 5-mL overnight
561 culture, and bacteria were grown in baffled Erlenmeyer flasks at 37°C and 225 rpm agitation. At an
562 optical density at 600 nm (OD_{600}) of around 0.7, the expression was induced by 1 mM isopropyl-β-
563 thiogalactopyranoside (IPTG), and 0.5 mM δ-aminolevulinic acid was added to support biliverdin
564 incorporation. The expression was performed at 16°C and 225 rpm agitation in darkness for around
565 65 h. All following steps were performed in green safe light. After harvesting the cells by
566 centrifugation, they were resuspended in lysis buffer [50 mM tris(hydroxy-methyl)-amino-methane
567 (Tris)/HCl, 20 mM NaCl, 10 mM imidazole, 1 mM β-mercaptoethanol, pH 8.0, protease inhibitor
568 completeOne (Roche), 1 mg mL^{-1} lysozyme]. Cells were lysed by sonification, and the supernatant of
569 the centrifuged lysate was applied to a HiTrap TALON crude column loaded with cobalt-
570 nitrilotriacetic resin (Cytiva). The column was washed with buffer [50 mM Tris/HCl, 20 mM NaCl, 1
571 mM β-mercaptoethanol, pH 8.0], and the His-tagged proteins were eluted by an imidazole gradient
572 from 0 to 0.5 M. Fractions were analyzed by denaturing SDS polyacrylamide gel electrophoresis
573 (PAGE) in the presence of 1 mM Zn^{2+} to visualize biliverdin incorporation (Berkelman and Lagarias,
574 1986) and pooled based on protein content. During an overnight dialysis at 4°C into buffer [50 mM
575 Tris/HCl, 20 mM NaCl, 1 mM β-mercaptoethanol, pH 8.0], the His-tag was cleaved off by His_6-tagged
576 TEV protease. The sample was applied twice to a gravity-flow IMAC column with HisPur cobalt resin
577 (ThermoFisher) using the same buffers as before. Cleavage of the His-tag and protein purity were
578 analyzed by Zn-SDS-PAGE. Fractions were pooled, dialyzed overnight at 4°C against storage buffer

579 [20 mM Tris/HCl, 20 mM NaCl, 10% (w/v) glycerol, 1 mM dithiothreitol, pH 8.0], concentrated via
580 spin filtration, and stored at -80°C.

581 **UV/vis Absorption Spectroscopy**

582 Absorption spectroscopy was carried out on a Cary60 UV/vis spectrophotometer (Agilent
583 Technologies) at 25°C under green safe light. Protein samples were diluted into buffers with pH
584 ranging from 6.0 to 11.0 (30 mM 2-(N-morpholino)ethanesulfonic acid/HCl, 30 mM NaCl, pH
585 6.0/6.5/7.0; 30 mM Tris/HCl, 30 mM NaCl, pH 7.5/8.0/8.5/9.0; 30 mM glycine/HCl, 30 mM NaCl, pH
586 10.0/10.5/11.0] (Rumfeldt et al., 2019). Samples were illuminated for 120 s with LEDs emitting in
587 the NIR [(800 ± 18) nm], red [(650 ± 10) nm] and blue [(470 ± 5) nm]. Data were normalized by the
588 Soret absorbance at 403 nm. Pr→Pfr dark recovery kinetics were monitored every 5 s at 760 nm and
589 fitted to single-exponential functions using the Fit-o-mat software (Möglich, 2018). Pr:Pfr ratios after
590 red or blue illumination were calculated via linear combination of the basis spectra as described
591 previously (Yi et al., 2025). The variation of photochemical parameters with pH was evaluated by
592 fitting to the Henderson-Hasselbalch equation. The ratio of the quantum yields Φ_p and Φ_q for the
593 red-light-driven photoconversion in the Pr→Pfr and Pfr→Pr directions, respectively (see Suppl. Fig.
594 1f), can be determined as follows (Yi et al., 2025):

595 $$\Phi_q/\Phi_p = P_R/P_{FR} \times (1 - 10^{-A_{Pr}})/(1 - 10^{-A_{Pfr}})$$

596 P_R and P_{FR} are the Pr and Pfr proportions at red-light-induced photostationary state, and A_{Pr} and A_{Pfr}
597 denote the absorbance in the Pr and Pfr states at the peak emission wavelength of the red-light
598 source.

599 **Generation and Screening of Linker Variants**

600 *Ac*NIRusk, *Av*NIRusk, *Dm*Ttr-REDusk and *Av*Tod-NIRusk linker variants were created with the PATCHY
601 strategy (Meier et al., 2024a; Ohlendorf et al., 2016). Sets of forward and reverse primers to generate

602 linker variants were designed using a custom Python script (https://github.com/vrylr/PATCHY). In
603 brief, PCR amplification was carried out using the primer sets in a final concentration of 0.25 µM.
604 After purifying the PCR product by gel extraction, the start constructs were digested with *Ksp*AI or
605 *Eco*32I (Suppl. Fig. 3, 6), followed by phosphorylation with T4 polynucleotide kinase and ligation with
606 T4 DNA ligase. The reaction mixes were transformed into DH10b cells and plated on LB plates
607 supplemented with kanamycin (LB/Kan). Plates were incubated overnight at 37°C in darkness, or
608 under red light [100 µW cm^{-2}, (650 ± 11) nm] or NIR light [200 µW cm^{-2}, (800 ± 18) nm]. Applied light
609 intensities were calibrated with a power meter (model 842-PE, equipped with a 918D-UV-OD3 silicon
610 photodiode, Newport, Darmstadt, Germany). Bacterial colonies developing red color upon overnight
611 incubation, indicative of *Ds*Red production, were used to inoculate 200 µL LB/Kan in a clear 96-well
612 microtiter plate (MTP) (Nunc, ThermoFisher). Bacteria were incubated for 21-24 h at 30°C and 750
613 rpm agitation. Next, the cultures were diluted 100-fold into fresh LB/Kan medium and split into three
614 separate cultures which were then incubated at 37°C and 750 rpm agitation in either darkness, red
615 light [100 µW cm^{-2}, (650 ± 11) nm], or NIR light [200 µW cm^{-2}, (800 ± 18) nm]. After 18 h, the optical
616 density at (600 ± 9) nm (OD_{600}) and the *Ds*Red fluorescence [(554 ± 9) nm excitation and (591 ± 20)
617 nm emission] were measured with a Tecan Infinite M200 Pro MTP reader (Tecan Group, Ltd.,
618 Männedorf, Switzerland). The *Ds*Red fluorescence was normalized by OD_{600} and represent the mean
619 ± s.d. of three biologically independent replicates.

620 **Light-Dose-Response Assays in *Escherichia coli***

621 Analyses were performed as before (Meier et al., 2024a; Multamäki et al., 2022). *E. coli* CmpX13
622 (Mathes et al., 2009) or *E. coli* Nissle (*Ec*N, DSMZ no. 115365) bacteria containing the respective
623 construct were used to inoculate 5 mL LB medium supplemented with 50 µg mL^{-1} Kan (LB/Kan) or
624 100 µg mL^{-1} Str (LB/Str). Cultures were incubated for 21-24 h at 30°C and 225 rpm agitation under
625 non-inducing light conditions. Under green safe light, the bacteria were diluted 100-fold into fresh

626 LB/Kan or LB/Str, before distributing 200 µL each into 64 wells of a black-walled MTP with clear
627 bottom (µClear, Greiner BioOne, Frickenhausen, Germany). As a control, bacteria harboring an
628 empty plasmid variant with a multiple-cloning site (MCS) were also placed on the MTP. After sealing
629 the MTP with a gas-permeable membrane, it was placed on an Arduino-controlled illumination
630 device. For the application of red and blue light, a previous setup was used (Hennemann et al., 2018)
631 with LED peak wavelengths of (624 ± 8) nm and (463 ± 12) nm, respectively. To apply NIR light, we
632 devised a new matrix of 8-by-8 LEDs emitting at (800 ± 18) nm (LED800-01AU, Roithner Lasertechnik)
633 which is controlled by an Arduino circuit board (Suppl. Fig. 4). The bacteria inside the MTPs were
634 incubated for 18 h at 37°C and 750 rpm agitation. The illumination was applied in 1:2 or 1:10 duty
635 cycles (i.e., 1 s light and 1 s darkness, or 20 s light and 180 s darkness). After incubation, the OD_{600}
636 and *Ds*Red fluorescence were determined as above. For measurements of YPet fluorescence,
637 excitation and emission wavelengths of (500 ± 9) nm and (554 ± 9) nm were used. Following
638 normalization to OD_{600}, the MCS background was subtracted. Data represent mean ± s.d. of three
639 biological replicates and were evaluated as a function of the light intensity averaged over the duty
640 cycle according to Hill isotherms using Fit-o-mat.

641 **Flow Cytometry**

642 *E. coli* CmpX13 cells (Mathes et al., 2009) containing *Ac*NIRusk, *Av*NIRusk, or an empty-vector control
643 (MCS) were analyzed by flow cytometry (Meier et al., 2024a). After overnight incubation for 21-24
644 h at 30°C and 750 rpm agitation, bacterial cultures were diluted 100-fold into fresh LB/Kan medium.
645 For each variant, the cultures were split and incubated for 18 h at 37°C and 750 rpm agitation in
646 either darkness, red light [100 µW cm^{-2}, (624 ± 8) nm], blue light [70 µW cm^{-2}, (463 ± 12) nm], or
647 different intensities (18-270 µW cm^{-2}) of NIR light [(800 ± 18) nm]. Following incubation, the cultures
648 were diluted 10-fold into phosphate-buffered saline (1x sheath fluid, Bio-Rad) and analyzed on a S3e
649 cell sorter (Bio-Rad). The *Ds*Red fluorescence of at least 200,000 events was detected using

650 excitation lasers at 488 nm and 561 nm and an emission channel at (585 ± 15) nm. Data were fitted
651 to skewed Gaussian distributions using Fit-o-mat. Experiments were repeated three times with
652 similar results.

653 **Growth and Expression Kinetics**

654 The growth and reporter-gene expression of *E. coli* CmpX13 cells (Mathes et al., 2009) containing
655 *Ac*NIRusk, *Av*NIRusk, or an empty-vector control (MCS) were analyzed over time as described before
656 (Multamäki et al., 2022). For each variant, two 5-mL LB/Kan cultures were inoculated and incubated
657 in darkness and under NIR light [200 µW cm^{-2}, (800 ± 18) nm] at 37°C and 600 rpm agitation. At
658 discrete times, samples of 200 µL were supplemented with 3.5 mg mL^{-1} chloramphenicol and 0.4 mg
659 mL^{-1} tetracycline to arrest cell growth and translation. After an incubation of at least 2 h, the OD_{600}
660 and *Ds*Red fluorescence were determined as above. Data represent mean ± s.d. of three biological
661 replicates and were fitted to logistic functions.

662 **Multiplexing of Optogenetic Circuits**

663 Pairs of plasmids harboring light-responsive TCSs were serially transformed into chemically
664 competent *E. coli* CmpX13. 200 µL LB supplemented with 50 µg mL^{-1} Kan and 100 µg mL^{-1} Str
665 (LB/Kan+Str) were inoculated with single bacterial clones and incubated for 21-24 h inside MTP wells
666 at 30°C and 750 rpm agitation in darkness. The cultures were then diluted 100-fold into LB/Kan+Str
667 before dispensation of 200 µL each into individual wells of four µClear MTPs. The MTPs were
668 incubated for 18 h at 37°C and 750 rpm agitation in either darkness, under red light [100 µW cm^{-2},
669 (624 ± 8) nm], NIR light [200 µW cm^{-2}, (800 ± 18) nm], or both light colors combined. Where
670 applicable, red light was applied continuously from below using the Arduino-controlled RGB LED
671 matrix, whereas NIR light shone from above. After 18 h incubation, the OD_{600}, and *Ds*Red and YPet
672 fluorescence were measured as above. Data represent mean ± s.d. of three biological replicates.

673 **Luciferase Assays in *Agrobacterium tumefaciens***

674 The *Dm*REDlux and *Av*NIRlux plasmids were transferred to *Agrobacterium tumefaciens* C58 (also
675 known as *Agrobacterium fabrum* C58, Lab collection, ATCC 33970) by biparental conjugation using
676 *E. coli* WM3064 as a diaminopimelic acid auxotrophic donor strain (William Metcalf, UIUC,
677 unpublished; *thrB1004 pro thi rpsL hsdS lacZ*Δ*M15* RP4-1360 *Δ(araBAD)567 ΔdapA1341::[erm pir*
678 *(wt)])*. Unless specified otherwise, C58 was routinely cultivated in LB medium at 28°C with 170 rpm
679 agitation. Selection for mini-Tn5 insertion mutants carrying the *lux* reporter constructs was carried
680 out on solid LB with 1.5% (w/v) agar and 50 µg mL^{-1} Kan. *E. coli* WM3064 strains carrying plasmids
681 were cultivated at 37°C with 200 rpm shaking in LB supplemented with 0.1 mM DL-a,e-
682 diaminopimelic acid (DAP) and 25 µg mL^{-1} Kan or 50 µg mL^{-1} ampicillin (Amp).

683 The protocol for biparental conjugation was described before (Dziuba et al., 2021). Briefly,
684 cultures of the C58 receptor and plasmid-containing *E. coli* strains were cultivated in LB or LB/Amp
685 medium overnight. Then, 2×10^9 cells of each strain were mixed in 15-mL falcon tubes and pelleted
686 at 5,421 g for 10 min. The supernatant was discarded while the cell pellet was resuspended in 100-
687 200 µL LB medium and spotted onto LB agar plates. After overnight incubation at 28°C, cells were
688 resuspended in 1 mL LB and transferred to 15-mL falcon tubes containing 9 mL LB medium. After
689 incubation for 2 h at 28°C and 120 rpm agitation, the cell suspension was pelleted by centrifugation,
690 and the supernatant was discarded. Following resuspension in 1 mL LB medium, 100 µL of 10- and
691 100-fold diluted cell suspensions were plated on LB-Kan agar plates. After incubation for three days
692 at 28°C, Kan-resistance plasmid insertion mutants were transferred to fresh LB/Kan agar plates and
693 screened by PCR.

694 At least three randomly selected transconjugants containing the luciferase reporter
695 constructs were analyzed for luminescence. Each experiment was performed in duplicate.
696 Luminescence signals, measured as arbitrary light units (ALU), were detected using a Tecan Infinite

697 M200 Pro MTP reader equipped with a luminometer module (Tecan Group, Ltd., Männedorf,
698 Switzerland) during culture growth in LB medium at 23°C and 280 rpm. Measurements were taken
699 every 20 minutes over 300 cycles (~90 h). ALU readings were normalized by the optical density at
700 650 nm (OD_{650}) to calculate the relative light units (RLU). To this end, tested clones were inoculated
701 into 600 µL LB/Kan medium in 24-well plates and incubated for ~ 20 h under non-inducing conditions
702 (i.e., red light for *Dm*REDlux and darkness for *Av*NIRlux, respectively) at 28°C and 140 rpm. Cultures
703 were then diluted 10-fold into 1 mL LB/Kan and incubated under identical conditions for an
704 additional 4-5 h. Subsequently, the OD_{650} was adjusted to 0.1 by adding fresh LB/Kan medium, and
705 100 µL of the normalized cell suspension was transferred into two 96-well MTPs. Cultivation of both
706 MTPs was initiated simultaneously, with one incubated under dark conditions and the other one
707 under red [(650 ± 11) nm] or NIR light [(800 ± 18) nm].

708 Alternatively, luminescence was assessed using a spotting assay. Precultures were prepared
709 as above, and 5 µL of the OD_{650}-normalized cell suspension were spotted onto LB/Kan agar plates.
710 The plates were incubated for 44 h at 28°C under dark conditions or under blue [(470 ± 13) nm], red
711 [(650 ± 11) nm], or NIR light [(800 ± 18) nm]. Luminescence signals were documented as cumulative
712 signal intensities using the Bio-Rad ChemiDoc XRS+ System (Bio Rad Laboratories Inc., Herkules,
713 USA), with images captured every 0.6 s over a 1-min period. In addition, colorimetric images were
714 acquired to visualize the outlines of the spotted cell suspensions. Luminescence was quantified from
715 the image time series by calculating the slope of the mean pixel intensities within the outlined cell
716 suspension areas using the Image J Fiji package (v1.54f) (Schindelin et al., 2012). Background
717 correction was performed by subtracting the mean pixel intensity of an uninoculated region of the
718 agar plate.

Data Availability

Data underlying the main and supplemental figures of the work are available at Zenodo (https://doi.org/10.5281/zenodo.16933397). The *Av*NIRusk plasmid is available from Addgene under accession number 235084. Additional materials are available from the corresponding author upon reasonable request.

References

Abramson J, Adler J, Dunger J, Evans R, Green T, Pritzel A, Ronneberger O, Willmore L, Ballard AJ, Bambrick J, Bodenstein SW, Evans DA, Hung C-C, O'Neill M, Reiman D, Tunyasuvunakool K, Wu Z, Žemgulytė A, Arvaniti E, Beattie C, Bertolli O, Bridgland A, Cherepanov A, Congreve M, Cowen-Rivers AI, Cowie A, Figurnov M, Fuchs FB, Gladman H, Jain R, Khan YA, Low CMR, Perlin K, Potapenko A, Savy P, Singh S, Stecula A, Thillaisundaram A, Tong C, Yakneen S, Zhong ED, Zielinski M, Žídek A, Bapst V, Kohli P, Jaderberg M, Hassabis D, Jumper JM. 2024. Accurate structure prediction of biomolecular interactions with AlphaFold 3. *Nature* **630**:493–500. doi:10.1038/s41586-024-07487-w

Andersen KR, Leksa NC, Schwartz TU. 2013. Optimized E. coli expression strain LOBSTR eliminates common contaminants from His-tag purification. *Prot Struct Funct Bioinf* **81**:1857–1861. doi:10.1002/prot.24364

Anthamatten D, Hennecke H. 1991. The regulatory status of the fixL- and fixJ-like genes in Bradyrhizobium japonicum may be different from that in Rhizobium meliloti. *Mol Gen Genet* **225**:38–48.

Ash C, Dubec M, Donne K, Bashford T. 2017. Effect of wavelength and beam width on penetration in light-tissue interaction using computational methods. *Lasers Med Sci* **32**:1909–1918. doi:10.1007/s10103-017-2317-4

742 Berkelman TR, Lagarias JC. 1986. Visualization of bilin-linked peptides and proteins in polyacrylamide
743 gels. *Anal Biochem* **156**:194–201.
744 Blum M, Andreeva A, Florentino LC, Chuguransky SR, Grego T, Hobbs E, Pinto BL, Orr A, Paysan-
745 Lafosse T, Ponamareva I, Salazar GA, Bordin N, Bork P, Bridge A, Colwell L, Gough J, Haft DH,
746 Letunic I, Llinares-López F, Marchler-Bauer A, Meng-Papaxanthos L, Mi H, Natale DA, Orengo CA,
747 Pandurangan AP, Piovesan D, Rivoire C, Sigrist CJA, Thanki N, Thibaud-Nissen F, Thomas PD,
748 Tosatto SCE, Wu CH, Bateman A. 2025. InterPro: the protein sequence classification resource in
749 2025. *Nucl Acids Res* **53**:D444–D456. doi:10.1093/nar/gkae1082
750 Bódizs S, Mészáros P, Grunewald L, Takala H, Westenhoff S. 2024. Cryo-EM structures of a bathy
751 phytochrome histidine kinase reveal a unique light-dependent activation mechanism. *Structure*
752 **32**:1952-1962.e3. doi:10.1016/j.str.2024.08.008
753 Böhm C, Lehtinen K, Multamäki E, Vanhatalo R, Brander O, Meier SSM, Rumfeldt JA, Möglich A,
754 Takala H. 2025. Traits and application of bathy phytochromes to bacterial optogenetics.
755 *submitted*.
756 Borucki B, von Stetten D, Seibeck S, Lamparter T, Michael N, Mroginski MA, Otto H, Murgida DH,
757 Heyn MP, Hildebrandt P. 2005. Light-induced proton release of phytochrome is coupled to the
758 transient deprotonation of the tetrapyrrole chromophore. *J Biol Chem* **280**:34358–64.
759 Burgie ES, Basore K, Rau MJ, Summers B, Mickles AJ, Grigura V, Fitzpatrick JAJ, Vierstra RD. 2024.
760 Signaling by a bacterial phytochrome histidine kinase involves a conformational cascade
761 reorganizing the dimeric photoreceptor. *Nat Commun* **15**:6853. doi:10.1038/s41467-024-50412-
762 y
763 Busch A, Guazzaroni M-E, Lacal J, Ramos JL, Krell T. 2009. The Sensor Kinase TodS Operates by a
764 Multiple Step Phosphorelay Mechanism Involving Two Autokinase Domains*. *J Biol Chem*
765 **284**:10353–10360. doi:10.1074/jbc.M900521200

766 Buschiazzo A, Trajtenberg F. 2019. Two-Component Sensing and Regulation: How Do Histidine
767 Kinases Talk with Response Regulators at the Molecular Level? *Annu Rev Micro* **73**:507–528.
768 doi:10.1146/annurev-micro-091018-054627
769 Chernov KG, Redchuk TA, Omelina ES, Verkhusha VV. 2017. Near-Infrared Fluorescent Proteins,
770 Biosensors, and Optogenetic Tools Engineered from Phytochromes. *Chem Rev* **117**:6423–6446.
771 doi:10.1021/acs.chemrev.6b00700
772 Cubillos-Ruiz A, Guo T, Sokolovska A, Miller PF, Collins JJ, Lu TK, Lora JM. 2021. Engineering living
773 therapeutics with synthetic biology. *Nat Rev Drug Discov* **20**:941–960. doi:10.1038/s41573-021-
774 00285-3
775 Cui M, Sun T, Li Shubin, Pan H, Liu J, Zhang X, Li L, Li Shanshan, Wei C, Yu C, Yang C, Ma N, Ma B, Lu
776 S, Chang J, Zhang W, Wang H. 2021. NIR light-responsive bacteria with live bio-glue coatings for
777 precise colonization in the gut. *Cell Rep* **36**:109690. doi:10.1016/j.celrep.2021.109690
778 Daeffler KN, Galley JD, Sheth RU, Ortiz-Velez LC, Bibb CO, Shroyer NF, Britton RA, Tabor JJ. 2017.
779 Engineering bacterial thiosulfate and tetrathionate sensors for detecting gut inflammation. *Mol*
780 *Syst Biol* **13**:923. doi:10.15252/msb.20167416
781 Davis SJ, Vener AV, Vierstra RD. 1999. Bacteriophytochromes: Phytochrome-Like Photoreceptors
782 from Nonphotosynthetic Eubacteria. *Science* **286**:2517–2520.
783 doi:10.1126/science.286.5449.2517
784 Deisseroth K, Feng G, Majewska AK, Miesenböck G, Ting A, Schnitzer MJ. 2006. Next-generation
785 optical technologies for illuminating genetically targeted brain circuits. *J Neurosci* **26**:10380–
786 10386. doi:10.1523/JNEUROSCI.3863-06.2006
787 Diensthuber RP, Bommer M, Gleichmann T, Möglich A. 2013. Full-length structure of a sensor
788 histidine kinase pinpoints coaxial coiled coils as signal transducers and modulators. *Structure*
789 **21**:1127–1136. doi:10.1016/j.str.2013.04.024

790 Dziuba M, Riese CN, Borgert L, Wittchen M, Busche T, Kalinowski J, Uebe R, Schüler D. 2021. The
791 Complex Transcriptional Landscape of Magnetosome Gene Clusters in Magnetospirillum
792 gryphiswaldense. *mSystems* **6**:10.1128/msystems.00893-21. doi:10.1128/msystems.00893-21
793 Etzl S, Lindner R, Nelson MD, Winkler A. 2018. Structure-guided design and functional
794 characterization of an artificial red light–regulated guanylate/adenylate cyclase for optogenetic
795 applications. *J Biol Chem* **293**:9078–9089. doi:10.1074/jbc.RA118.003069
796 Gao R, Bouillet S, Stock AM. 2019. Structural Basis of Response Regulator Function. *Annu Rev Micro*
797 **73**:175–197. doi:10.1146/annurev-micro-020518-115931
798 Gibson DG, Young L, Chuang R-Y, Venter JC, Hutchison CA, Smith HO. 2009. Enzymatic assembly of
799 DNA molecules up to several hundred kilobases. *Nat Methods* **6**:343–345.
800 doi:10.1038/nmeth.1318
801 Gourinchas G, Etzl S, Göbl C, Vide U, Madl T, Winkler A. 2017. Long-range allosteric signaling in red
802 light-regulated diguanylyl cyclases. *Sci Adv* **3**:e1602498. doi:10.1126/sciadv.1602498
803 Hamblin MR. 2016. Shining light on the head: Photobiomodulation for brain disorders. *BBA Clinical*
804 **6**:113–124. doi:10.1016/j.bbacli.2016.09.002
805 Hartsough LA, Park M, Kotlajich MV, Lazar JT, Han B, Lin C-CJ, Musteata E, Gambill L, Wang MC, Tabor
806 JJ. 2020. Optogenetic control of gut bacterial metabolism to promote longevity. *Elife* **9**:e56849.
807 doi:10.7554/eLife.56849
808 Hennemann J, Iwasaki RS, Grund TN, Diensthuber RP, Richter F, Möglich A. 2018. Optogenetic Control
809 by Pulsed Illumination. *Chembiochem* **19**:1296–1304. doi:10.1002/cbic.201800030
810 Huber C, Strack M, Schultheiß I, Pielage J, Mechler X, Hornbogen J, Diller R, Frankenberg-Dinkel N.
811 2024. Darkness inhibits autokinase activity of bacterial bathy phytochromes. *J Biol Chem*
812 **300**:107148. doi:10.1016/j.jbc.2024.107148
813 Hughes J, Lamparter T, Mittmann F, Hartmann E, Gärtner W, Wilde A, Börner T. 1997. A prokaryotic
814 phytochrome. *Nature* **386**:663. doi:10.1038/386663a0

815 Hughes J, Winkler A. 2024. New Insight Into Phytochromes: Connecting Structure to Function. *Annu*
816 *Rev Plant Biol* **75**:153–183. doi:10.1146/annurev-arplant-070623-110636
817 Jacob-Dubuisson F, Mechaly A, Betton J-M, Antoine R. 2018. Structural insights into the signalling
818 mechanisms of two-component systems. *Nat Rev Micro* **16**:585. doi:10.1038/s41579-018-0055-
819 7
820 Jayaraman P, Devarajan K, Chua TK, Zhang H, Gunawan E, Poh CL. 2016. Blue light-mediated
821 transcriptional activation and repression of gene expression in bacteria. *Nucl Acids Res* **44**:6994–
822 7005. doi:10.1093/nar/gkw548
823 Jenal U, Reinders A, Lori C. 2017. Cyclic di-GMP: second messenger extraordinaire. *Nat Rev Microbiol*
824 **15**:271–284. doi:10.1038/nrmicro.2016.190
825 Karniol B, Vierstra RD. 2003. The pair of bacteriophytochromes from Agrobacterium tumefaciens are
826 histidine kinases with opposing photobiological properties. *Proc Natl Acad Sci U S A* **100**:2807–
827 2812. doi:10.1073/pnas.0437914100
828 Krell T, Lacal J, Busch A, Silva-Jiménez H, Guazzaroni M-E, Ramos JL. 2010. Bacterial Sensor Kinases:
829 Diversity in the Recognition of Environmental Signals. *Annu Rev Micro* **64**:539–559.
830 doi:10.1146/annurev.micro.112408.134054
831 Lamparter T, Michael N, Mittmann F, Esteban B. 2002. Phytochrome from Agrobacterium
832 tumefaciens has unusual spectral properties and reveals an N-terminal chromophore
833 attachment site. *Proc Natl Acad Sci U S A* **99**:11628–11633. doi:10.1073/pnas.152263999
834 Landry BP, Palanki R, Dyulgyarov N, Hartsough LA, Tabor JJ. 2018. Phosphatase activity tunes two-
835 component system sensor detection threshold. *Nat Commun* **9**:1433. doi:10.1038/s41467-018-
836 03929-y
837 Lau PCK, Wang Y, Patel A, Labbé D, Bergeron H, Brousseau R, Konishi Y, Rawlings M. 1997. A bacterial
838 basic region leucine zipper histidine kinase regulating toluene degradation. *Proc Natl Acad Sci U*
839 *S A* **94**:1453–1458. doi:10.1073/pnas.94.4.1453

840 Laub MT, Goulian M. 2007. Specificity in Two-Component Signal Transduction Pathways. *Annu Rev*
841 *Genet* **41**:121–145. doi:10.1146/annurev.genet.41.042007.170548
842 Lazar JT, Tabor JJ. 2021. Bacterial two-component systems as sensors for synthetic biology
843 applications. *Curr Opin Syst Biol* **28**:100398. doi:10.1016/j.coisb.2021.100398
844 Lehtinen K, Nokia MS, Takala H. 2022. Red Light Optogenetics in Neuroscience. *Front Cell Neurosci*
845 **15**.
846 Leopold AV, Chernov KG, Shemetov AA, Verkhusha VV. 2019. Neurotrophin receptor tyrosine kinases
847 regulated with near-infrared light. *Nat Commun* **10**:1–13. doi:10.1038/s41467-019-08988-3
848 Leopold AV, Thankachan S, Yang C, Gerashchenko D, Verkhusha VV. 2022. A general approach for
849 engineering RTKs optically controlled with far-red light. *Nat Methods* **19**:871–880.
850 doi:10.1038/s41592-022-01517-z
851 Levskaya A, Chevalier AA, Tabor JJ, Simpson ZB, Lavery LA, Levy M, Davidson EA, Scouras A, Ellington
852 AD, Marcotte EM, Voigt CA. 2005. Synthetic biology: Engineering Escherichia coli to see light.
853 *Nature* **438**:441–442. doi:10.1038/nature04405
854 Liu W, Yuan JS, Stewart Jr CN. 2013. Advanced genetic tools for plant biotechnology. *Nat Rev Genet*
855 **14**:781–793. doi:10.1038/nrg3583
856 Magaraci MS, Veerakumar A, Qiao P, Amurthur A, Lee JY, Miller JS, Goulian M, Sarkar CA. 2014.
857 Engineering Escherichia coli for Light-Activated Cytolysis of Mammalian Cells. *ACS Synth Biol*
858 **3**:944–948. doi:10.1021/sb400174s
859 Malla TN, Hernandez C, Muniyappan S, Menendez D, Bizhga D, Mendez JH, Schwander P, Stojković
860 EA, Schmidt M. 2024. Photoreception and signaling in bacterial phytochrome revealed by single-
861 particle cryo-EM. *Sci Adv* **10**:eadq0653. doi:10.1126/sciadv.adq0653
862 Mathes T, Vogl C, Stolz J, Hegemann P. 2009. In vivo generation of flavoproteins with modified
863 cofactors. *J Mol Biol* **385**:1511–1518. doi:10.1016/j.jmb.2008.11.001

Meier SSM, Multamäki E, Ranzani AT, Takala H, Möglich A. 2024a. Leveraging the histidine kinase-phosphatase duality to sculpt two-component signaling. *Nat Commun* **15**:4876. doi:10.1038/s41467-024-49251-8

Meier SSM, Multamäki E, Ranzani AT, Takala H, Möglich A. 2024b. Multimodal Control of Bacterial Gene Expression by Red and Blue Light. *Meth Mol Biol* **2760**:463–477. doi:10.1007/978-1-0716-3658-9_26

Möglich A. 2019. Signal transduction in photoreceptor histidine kinases. *Prot Sci* **28**:1923–1946. doi:10.1002/pro.3705

Möglich A. 2018. An Open-Source, Cross-Platform Resource for Nonlinear Least-Squares Curve Fitting. *J Chem Educ* **95**:2273–2278. doi:10.1021/acs.jchemed.8b00649

Möglich A, Ayers RA, Moffat K. 2010. Addition at the molecular level: signal integration in designed Per-ARNT-Sim receptor proteins. *J Mol Biol* **400**:477–486. doi:10.1016/j.jmb.2010.05.019

Möglich A, Ayers RA, Moffat K. 2009. Design and signaling mechanism of light-regulated histidine kinases. *J Mol Biol* **385**:1433–1444. doi:10.1016/j.jmb.2008.12.017

Mukougawa K, Kanamoto H, Kobayashi T, Yokota A, Kohchi T. 2006. Metabolic engineering to produce phytochromes with phytochromobilin, phycocyanobilin, or phycoerythrobilin chromophore in Escherichia coli. *FEBS Lett* **580**:1333–1338. doi:10.1016/j.febslet.2006.01.051

Multamäki E, García de Fuentes A, Sieryi O, Bykov A, Gerken U, Ranzani AT, Köhler J, Meglinski I, Möglich A, Takala H. 2022. Optogenetic Control of Bacterial Expression by Red Light. *ACS Synth Biol* **11**:3354–3367. doi:10.1021/acssynbio.2c00259

Multamäki E, Nanekar R, Morozov D, Lievonen T, Golonka D, Wahlgren WY, Stucki-Buchli B, Rossi J, Hytönen VP, Westenhoff S, Ihalainen JA, Möglich A, Takala H. 2021. Comparative analysis of two paradigm bacteriophytochromes reveals opposite functionalities in two-component signaling. *Nat Commun* **12**:4394. doi:10.1038/s41467-021-24676-7

888 Nguyen AW, Daugherty PS. 2005. Evolutionary optimization of fluorescent proteins for intracellular
889 FRET. *Nat Biotechnol* **23**:355–360. doi:10.1038/nbt1066
890 Ohlendorf R, Möglich A. 2022. Light-regulated gene expression in Bacteria: Fundamentals, advances,
891 and perspectives. *Front Bioeng Biotech* **10**:1029403.
892 Ohlendorf R, Schumacher CH, Richter F, Möglich A. 2016. Library-Aided Probing of Linker
893 Determinants in Hybrid Photoreceptors. *ACS Synth Biol* **5**:1117–1126.
894 doi:10.1021/acssynbio.6b00028
895 Ohlendorf R, Vidavski RR, Eldar A, Moffat K, Möglich A. 2012. From dusk till dawn: one-plasmid
896 systems for light-regulated gene expression. *J Mol Biol* **416**:534–542.
897 doi:10.1016/j.jmb.2012.01.001
898 Ong NT, Olson EJ, Tabor JJ. 2018. Engineering an E. coli Near-Infrared Light Sensor. *ACS Synth Biol*
899 **7**:240–248. doi:10.1021/acssynbio.7b00289
900 Pan H, Li L, Pang G, Han C, Liu B, Zhang Y, Shen Y, Sun T, Liu J, Chang J, Wang H. 2021. Engineered NIR
901 light-responsive bacteria as anti-tumor agent for targeted and precise cancer therapy. *Chem Eng*
902 *J* **426**:130842. doi:10.1016/j.cej.2021.130842
903 Parkinson JS, Kofoid EC. 1992. Communication Modules in Bacterial Signaling Proteins. *Annu Rev*
904 *Genet* **26**:71–112. doi:10.1146/annurev.ge.26.120192.000443
905 Ramos-González M-I, Olson M, Gatenby AA, Mosqueda G, Manzanera M, Campos MJ, Víchez S,
906 Ramos JL. 2002. Cross-Regulation between a Novel Two-Component Signal Transduction System
907 for Catabolism of Toluene in Pseudomonas mendocina and the TodST System from Pseudomonas
908 putida. *J Bact* **184**:7062–7067. doi:10.1128/jb.184.24.7062-7067.2002
909 Ranzani AT, Buchholz K, Blackholm M, Kopkin H, Möglich A. 2024. Induction of bacterial expression
910 at the mRNA level by light. *Nucl Acids Res* **52**:10017–10028. doi:10.1093/nar/gkae678
911 Rottwinkel G, Oberpichler I, Lamparter T. 2010. Bathy Phytochromes in Rhizobial Soil Bacteria. *J Bact*
912 **192**:5124–5133. doi:10.1128/JB.00672-10

913 Rumfeldt JA, Takala H, Liukkonen A, Ihalainen JA. 2019. UV-Vis Spectroscopy Reveals a Correlation
914 Between Y263 and BV Protonation States in Bacteriophytochromes. *Photochem Photobiol*
915 **95**:969–979. doi:https://doi.org/10.1111/php.13095
916 Russo FD, Silhavy TJ. 1993. The essential tension: opposed reactions in bacterial two-component
917 regulatory systems. *Trends Microbiol* **1**:306–310.
918 Sankaran S, del Campo A. 2019. Optoregulated Protein Release from an Engineered Living Material.
919 *Adv Biosyst* **3**:1800312. doi:10.1002/adbi.201800312
920 Schindelin J, Arganda-Carreras I, Frise E, Kaynig V, Longair M, Pietzsch T, Preibisch S, Rueden C,
921 Saalfeld S, Schmid B, Tinevez J-Y, White DJ, Hartenstein V, Eliceiri K, Tomancak P, Cardona A. 2012.
922 Fiji: an open-source platform for biological-image analysis. *Nat Methods* **9**:676–682.
923 doi:10.1038/nmeth.2019
924 Schmidl SR, Sheth RU, Wu A, Tabor JJ. 2014. Refactoring and Optimization of Light-Switchable
925 Escherichia coli Two-Component Systems. *ACS Synth Biol* **3**:820–831. doi:10.1021/sb500273n
926 Schmidt A, Sauthof L, Szczepek M, Lopez MF, Escobar FV, Qureshi BM, Michael N, Buhrke D, Stevens
927 T, Kwiatkowski D, von Stetten D, Mroginski MA, Krauß N, Lamparter T, Hildebrandt P, Scheerer P.
928 2018. Structural snapshot of a bacterial phytochrome in its functional intermediate state. *Nat*
929 *Commun* **9**:4912. doi:10.1038/s41467-018-07392-7
930 Silva-Jiménez H, Ramos JL, Krell T. 2012. Construction of a prototype two-component system from
931 the phosphorelay system TodS/TodT. *Protein Eng Des Sel* **25**:159–169.
932 doi:10.1093/protein/gzs001
933 Stabel R, Stüven B, Hansen JN, Körschen HG, Wachten D, Möglich A. 2019. Revisiting and Redesigning
934 Light-Activated Cyclic-Mononucleotide Phosphodiesterases. *J Mol Biol* **431**:3029–3045.
935 doi:10.1016/j.jmb.2019.07.011

936 Strack RL, Strongin DE, Bhattacharyya D, Tao W, Berman A, Broxmeyer HE, Keenan RJ, Glick BS. 2008.
937 A noncytotoxic DsRed variant for whole-cell labeling. *Nat Methods* **5**:955–957.
938 doi:10.1038/nmeth.1264
939 Stüven B, Stabel R, Ohlendorf R, Beck J, Schubert R, Möglich A. 2019. Characterization and
940 engineering of photoactivated adenylyl cyclases. *Biol Chem* **400**:429–441. doi:10.1515/hsz-
941 2018-0375
942 Tabor JJ, Levskaya A, Voigt CA. 2011. Multichromatic control of gene expression in Escherichia coli. *J*
943 *Mol Biol* **405**:315–324. doi:10.1016/j.jmb.2010.10.038
944 Takala H, Edlund P, Ihalainen JA, Westenhoff S. 2020. Tips and turns of bacteriophytochrome
945 photoactivation. *Photochem Photobiol Sci* **19**:1488–1510. doi:10.1039/D0PP00117A
946 Tang K, Beyer HM, Zurbriggen MD, Gärtner W. 2021. The Red Edge: Bilin-Binding Photoreceptors as
947 Optogenetic Tools and Fluorescence Reporters. *Chem Rev* **121**:14906–14956.
948 doi:10.1021/acs.chemrev.1c00194
949 Tasler R, Moises T, Frankenberg-Dinkel N. 2005. Biochemical and spectroscopic characterization of
950 the bacterial phytochrome of Pseudomonas aeruginosa. *FEBS J* **272**:1927–1936.
951 doi:10.1111/j.1742-4658.2005.04623.x
952 Velazquez Escobar F, Piwowarski P, Salewski J, Michael N, Fernandez Lopez M, Rupp A, Qureshi BM,
953 Scheerer P, Bartl F, Frankenberg-Dinkel N, Siebert F, Andrea Mroginski M, Hildebrandt P. 2015. A
954 protonation-coupled feedback mechanism controls the signalling process in bathy
955 phytochromes. *Nature Chem* **7**:423–430. doi:10.1038/nchem.2225
956 Weissleder R. 2001. A clearer vision for *in vivo* imaging. *Nat Biotech* **19**:316–317. doi:10.1038/86684
957 Xu Q, Vogt A, Frechen F, Yi C, Küçükerden M, Ngum N, Sitjà-Roqueta L, Greiner A, Parri R, Masana M,
958 Wenger N, Wachten D, Möglich A. 2024. Engineering Bacteriophytochrome-coupled
959 Photoactivated Adenylyl Cyclases for Enhanced Optogenetic cAMP Modulation. *J Mol Biol*,
960 Photosensory Receptors-Mechanisms and Effects **436**:168257. doi:10.1016/j.jmb.2023.168257

961 Yang C, Cui M, Zhang Y, Pan H, Liu J, Wang S, Ma N, Chang J, Sun T, Wang H. 2020. Upconversion
962 optogenetic micro-nanosystem optically controls the secretion of light-responsive bacteria for
963 systemic immunity regulation. *Commun Biol* **3**:1–14. doi:10.1038/s42003-020-01287-4
964 Yang X, Kuk J, Moffat K. 2008. Crystal structure of Pseudomonas aeruginosa bacteriophytochrome:
965 Photoconversion and signal transduction. *Proc Natl Acad Sci U S A* **105**:14715–14720.
966 Yi C, Meier SSM, Kehr M, Möglich A. 2025. Spectroscopic Analyses of Photoconversion in
967 Phytochromes. *Meth Mol Biol* **submitted**.
968 Ziegler T, Möglich A. 2015. Photoreceptor engineering. *Front Mol Biosci* **2**:30.
969 doi:10.3389/fmolb.2015.00030
970 Zienicke B, Molina I, Glenz R, Singer P, Ehmer D, Escobar FV, Hildebrandt P, Diller R, Lamparter T.
971 2013. Unusual Spectral Properties of Bacteriophytochrome Agp2 Result from a Deprotonation
972 of the Chromophore in the Red-absorbing Form Pr*. *J Biol Chem* **288**:31738–31751.
973 doi:10.1074/jbc.M113.479535

974 **Acknowledgements**

975 We thank our colleagues for discussion; Dr. Roman S. Iwasaki, Dr. Ralph P. Diensthuber, and Tobias
976 von Basse for preliminary experiments; Tino Krell for generously providing the pMIR66 and pMIR77
977 plasmids; and Mr. Braun and the electronical workshop at University Bayreuth for support. Funding
978 was provided by the European Commission (FET Open NEUROPA grant 863214 to A.M.); the German
979 Research Foundation (grants MO2192/4-2 to A.M. and UE200/1-1 to R.U.); and the Research Council
980 of Finland (grant 330678 to H.T.).

981 **Author Contributions**

982 S.S.M.M. and A.M. conceived of the project; H.T., R.U., and A.M. acquired funding; S.S.M.M., M.H.,
983 C.B., R.U., and A.M. designed research; S.S.M.M., M.H., C.B., E.L.R.D., R.U., and A.M. conducted

research; S.S.M.M., M.H., C.B., E.L.R.D., R.U., and A.M. analyzed data; S.S.M.M. and A.M. wrote the manuscript; all authors edited the manuscript.

Competing Interests

The authors declare no competing interests.

Figure Legends

Figure 1

Spectroscopic characterization of bacteriophytochrome photosensory core modules (PCM) from *Azorhizobium caulinodans* (*Ac*PCM), *Agrobacterium vitis* (*Av*PCM), and *Pseudomonas aeruginosa* (*Pa*PCM). (a) UV/vis absorbance spectra of *Ac*PCM at pH 8 in darkness (black line), and after illumination with near-infrared (NIR, purple line), red (red), and blue light (blue). Data are normalized by the absorbance at 403 nm within the Soret band. The lower panel shows the NIR-dark difference absorbance spectrum with maxima and minima marked. (b) and (c) as in (a) but for *Av*PCM and *Pa*PCM. (d) Absorbance spectra of *Ac*PCM in darkness (solid lines) and after NIR illumination (dashed lines) at different pH values as indicated by color. (e) and (f) as in (d) but for *Av*PCM and *Pa*PCM. (g) Absorbance at 700 nm for *Ac*PCM (light purple circles), *Av*PCM (dark green squares), and *Pa*PCM (orange triangles) upon NIR-light exposure at different pH values. Data were fitted to the Henderson-Hasselbalch equation to determine apparent pK_a values (dashed lines, *Ac*PCM: 7.2 ± 0.1, *Av*PCM: 8.0 ± 0.1, *Pa*PCM: 9.9 ± 0.2). (h) Calculated Pfr fractions of *Ac*PCM (light purple circles), *Av*PCM (dark green square), and *Pa*PCM (orange triangles) after red-light exposure at different pH values. The underlying absorbance spectra are shown in Suppl. Fig. 1a-c. (i) Dark-recovery kinetics at 25°C and pH 8 after NIR-illumination as followed by absorbance at 760 nm. Time constants for *Ac*PCM (light purple), *Av*PCM (dark green), and *Pa*PCM (orange) were determined by single-exponential fits.

1006 **Figure 2**

1007 Engineering of light-regulated sensor histidine kinases (SHK) based on photosensory core modules
1008 (PCM) from bathy-bacteriophytochromes (BphP). (a) Schematic of the pNIRusk plasmids to control
1009 gene expression in bacteria by NIR light. The $LacI^q$ promoter constitutively expresses a tricistronic
1010 operon consisting of heme oxygenase (HO1), the light-regulated SHK (chimera of *Ac*/*Av*PCM and
1011 FixL), and the response regulator FixJ. When phosphorylated, FixJ binds to the FixK2 promoter and
1012 triggers the expression of a gene of interest (GOI). (b) Response of select *Ac*NIRusk (left) and
1013 *Av*NIRusk (right) systems to different light conditions (grey: darkness; purple: NIR light; red: red
1014 light). *Ds*Red reporter fluorescence was normalized by the optical density of the bacterial cultures.
1015 Individual pNIRusk variants are denoted by the relative lengths of the linkers within their underlying
1016 SHKs (see Suppl. Fig. 3), with the variants chosen for further analyses highlighted in bold. As control,
1017 an empty-vector construct (MCS) is shown, and data are normalized by the reference fluorescence
1018 value determined for the *Av*+17a variant. (c) Flow-cytometric analyses of bacteria containing
1019 *Ac*NIRusk-1a (top) or *Av*NIRusk+17a (bottom) upon incubation in darkness (black), blue (blue, 70 µW
1020 cm^{-2}), red (red, 100 µW cm^{-2}), or NIR light (purple, 200 µW cm^{-2}). An empty-vector control (MCS) is
1021 shown in green. (d) Light-dose response of bacteria containing *Ac*NIRusk-1a incubated in NIR (purple
1022 circles), red (red squares), and blue light (blue pentagons). (e) as in (d) but for *Av*NIRusk+17a.

1023 **Figure 3**

1024 Engineering of orthogonal light-regulated two-component systems (TCS). (a) Schematic of the
1025 *Dm*Ttr-REDusk circuit based on the TtrSR TCS from *Shewanella baltica* combined with the
1026 photosensory core module (PCM) from the *Deinococcus maricopensis* bacteriophytochrome (BphP)
1027 (top). Reporter fluorescence of bacteria bearing circuits with different linker lengths of their
1028 underlying sensor histidine kinases (SHK) upon cultivation in darkness (grey), NIR (purple), and red
1029 light (red) (bottom). An empty-vector control is denoted as 'MCS', and data are normalized as in Fig.

1030 2. Variants are marked by the relative lengths of the linkers within their underlying SHKs compared
1031 to pREDusk (see Suppl. Fig. 6). Variants characterized further are highlighted in bold. (b) as in (a) but
1032 for the *Av*Tod-NIRusk circuit based on the TodST TCS from *Pseudomonas putida* combined with the
1033 BphP PCM from *Agrobacterium vitis*. (c) Multiplexing of bacteria containing two optogenetic circuits,
1034 as noted below the graph, to separately control the expression of *Ds*Red (top) and YPet (bottom)
1035 reporters. After incubation in darkness (gray), NIR (purple), red (red), and combined NIR and red
1036 light (red and purple stripes), fluorescence was measured and, in the case of *Ds*Red, normalized as
1037 in Fig. 2. YPet fluorescence was normalized by the reference value determined for *Dm*REDusk-YPet
1038 under red light (this panel).

1039 **Figure 4**

1040 Light-regulated gene expression in *Escherichia coli* Nissle (*Ec*N) and *Agrobacterium tumefaciens*. (a)
1041 Light-dose response of *Ec*N harboring *Av*NIRusk after incubation at varying NIR-light (purple circles),
1042 red-light (red squares), and blue-light (blue pentagons) intensities. Corresponding data for *Ac*NIRusk
1043 are shown in Suppl. Fig. 8. (b) Schematic of the *Av*NIRlux and *Dm*REDlux circuits based on *Av*PCM
1044 and *Dm*PCM. The tricistronic cassette comprising heme oxygenase (HO1), the sensor histidine kinase
1045 (chimera of *Av*/*Dm*PCM and FixL), and FixJ is controlled by the constitutive PmamDC promoter from
1046 *Magnetospirillum gryphiswaldense*, whereas the FixK2 promoter regulates the expression of the
1047 *luxABCDE* operon. (c) *A. tumefaciens* bacteria bearing *Av*NIRlux (left) and *Dm*REDlux (right) were
1048 spotted on plates and incubated at different light conditions (darkness, NIR, red, or blue light),
1049 followed by luminescence (Lumi.) measurements (see Suppl. Fig. 9a). (d) *A. tumefaciens* bacteria
1050 carrying *Av*NIRlux and *Dm*REDlux were incubated in liquid culture for 20 h under different light
1051 conditions (gray: darkness, purple: NIR light, red: red light), followed by recording of reporter
1052 luminescence (see Suppl. Fig. 9c-d).

1053 **Figure 5**

1054 Photoreception by select bathy-bacteriophytochromes (BphP) at different pH values. Throughout
1055 the entire tested pH range, the photosensory core modules (PCM) of the bathy-BphPs from
1056 *Azorhizobium caulinodans* (*Ac*PCM), *Agrobacterium vitis* (*Av*PCM), and *Pseudomonas aeruginosa*
1057 (*Pa*PCM) adopt a pure Pfr state in darkness with fully protonated biliverdin (BV) chromophore. NIR
1058 light drives the complete conversion to the Pr state in which BV can be either protonated or
1059 deprotonated as governed by pH and the respective pK_a value of the bathy-BphP. Red light populates
1060 a photostationary mixture with Pr and Pfr proportions strongly depending on pH. At high pH values,
1061 red light can drive the bathy-BphP nearly completely to the Pr state for *Ac*PCM and *Av*PCM. Owing
1062 to a higher pK_a value for BV protonation, *Pa*PCM is less affected but follows the same trend.

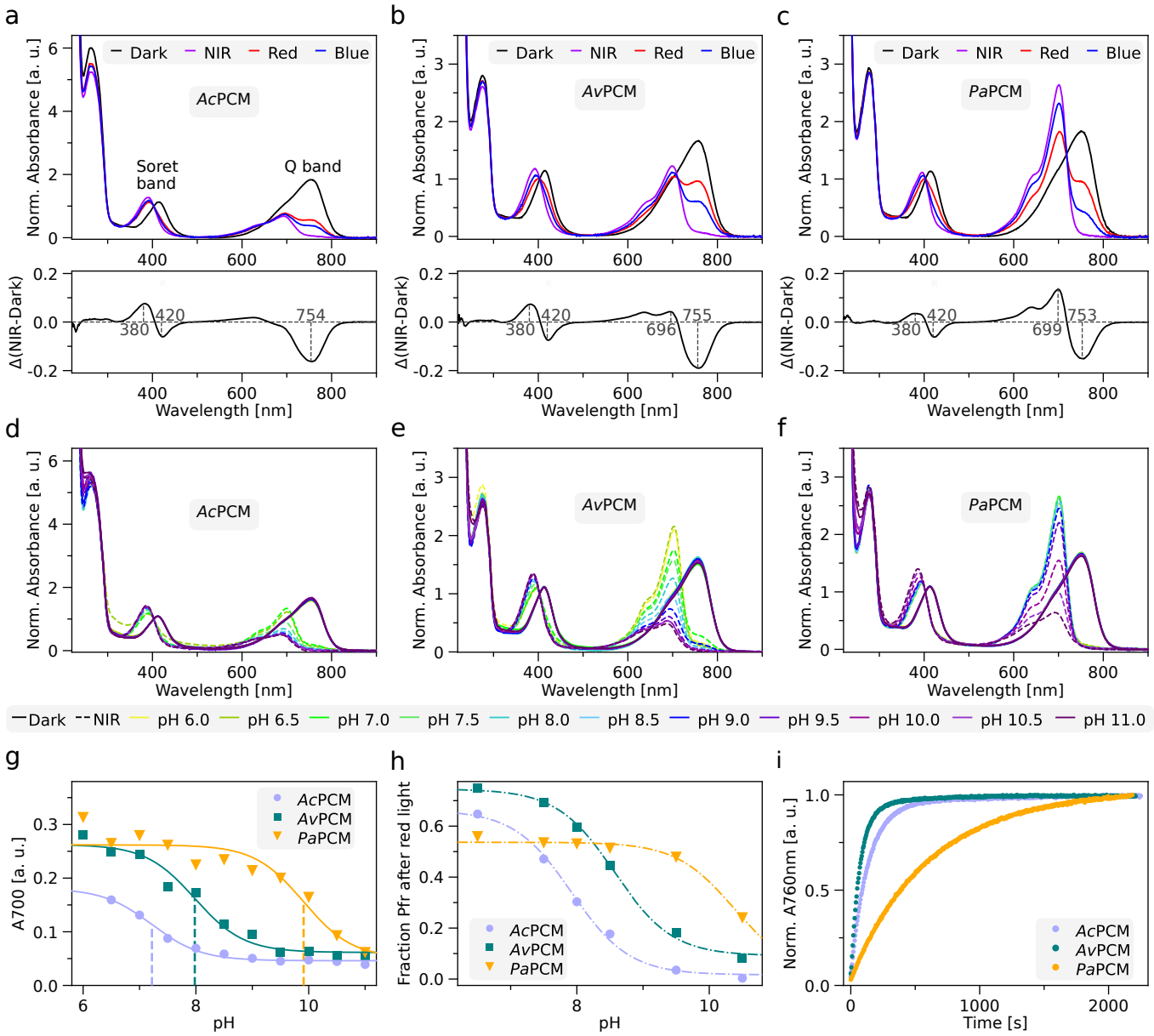
a
b
c
Dark
NIR
Red
Blue
AcPCM
AvPCM
PaPCM
Soret band
Q band
Norm. Absorbance [a. u.]
Δ(NIR-Dark)
380
420
754
755
696
753
699
Wavelength [nm]
d
e
f
Dark
NIR
pH 6.0
pH 6.5
pH 7.0
pH 7.5
pH 8.0
pH 8.5
pH 9.0
pH 9.5
pH 10.0
pH 10.5
pH 11.0
g
h
i
A700 [a. u.]
pH
Fraction Pfr after red light
Norm. A760nm [a. u.]
Time [s]

Figure 1

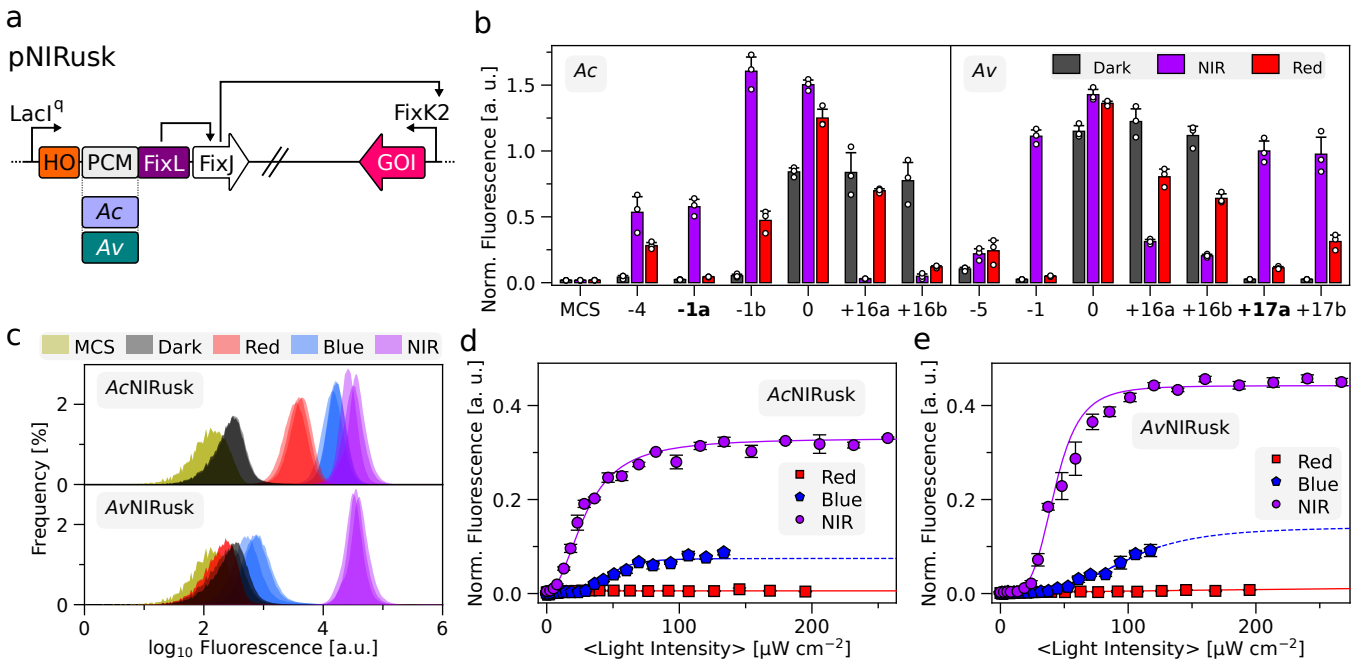
a
pNIRusk
LacI^q
FixK2
HO
PCM
FixL
FixJ
GOI
Ac
Av
b
Ac
Av
Dark
NIR
Red
Norm. Fluorescence [a. u.]
MCS
-4
-1a
-1b
0
+16a
+16b
-5
-1
+17a
+17b
c
MCS
Dark
Red
Blue
NIR
AcNIRusk
AvNIRusk
Frequency [%]
log10 Fluorescence [a.u.]
d
AcNIRusk
Red
Blue
NIR
Norm. Fluorescence [a. u.]
<Light Intensity> [μW cm^{-2}]
e
AvNIRusk
Red
Blue
NIR
Norm. Fluorescence [a. u.]
<Light Intensity> [μW cm^{-2}]

Figure 2

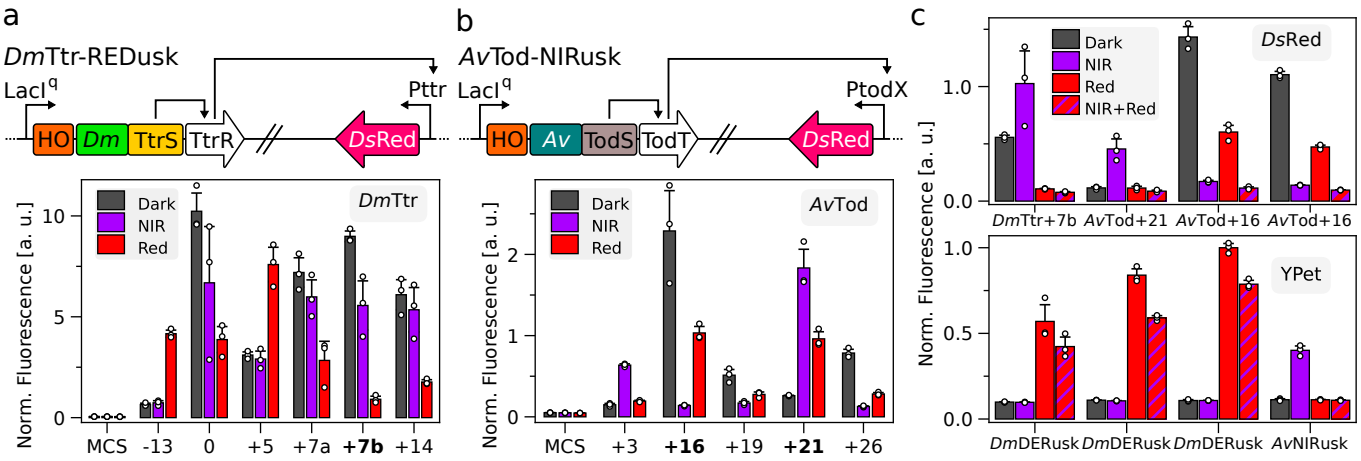
a
DmTtr-REDusk
LacI^q
Pttr
HO
Dm
TtrS
TtrR
DsRed
Dark
NIR
Red
DmTtr
Norm. Fluorescence [a. u.]
MCS
-13
0
+5
+7a
+7b
+14
b
AvTod-NIRusk
LacI^q
PtodX
HO
Av
TodS
TodT
DsRed
Dark
NIR
Red
AvTod
Norm. Fluorescence [a. u.]
MCS
+3
+16
+19
+21
+26
c
Dark
NIR
Red
NIR+Red
DsRed
Norm. Fluorescence [a. u.]
DmTtr+7b
AvTod+21
AvTod+16
AvTod+16
YPet
DmDERusk
DmDERusk
DmDERusk
AvNIRusk

Figure 3

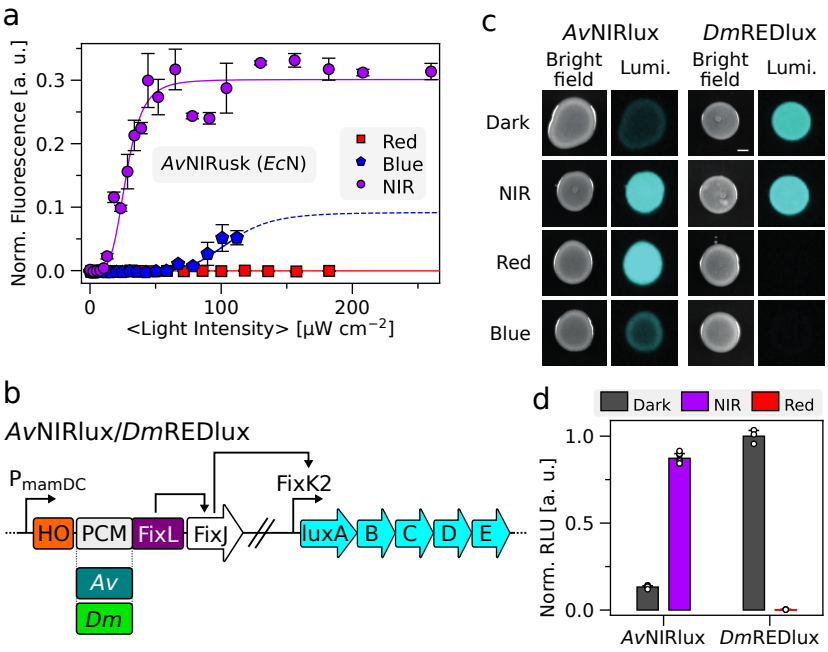
a
Norm. Fluorescence [a. u.]
0.3
0.2
0.1
0.0
0
100
200
<Light Intensity> [μW cm−2]
AvNIRusk (EcN)
Red
Blue
NIR
c
AvNIRlux
DmREDlux
Bright field
Lumi.
Bright field
Lumi.
Dark
NIR
Red
Blue
b
AvNIRlux/DmREDlux
PmamDC
HO
PCM
FixL
FixJ
FixK2
luxA
B
C
D
E
Av
Dm
d
Dark
NIR
Red
Norm. RLU [a. u.]
1.0
0.5
0.0
AvNIRlux
DmREDlux

Figure 4

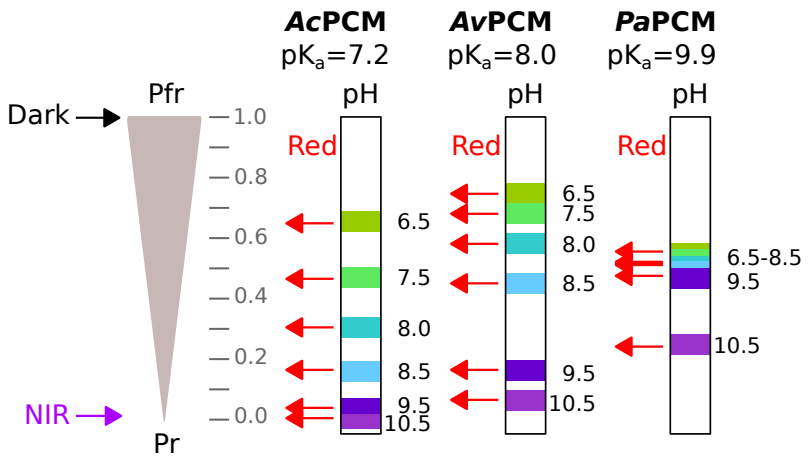
AcPCM
pKa=7.2
AvPCM
pKa=8.0
PaPCM
pKa=9.9
pH
pH
pH
Dark
Pfr
NIR
Pr
1.0
0.8
0.6
0.4
0.2
0.0
Red
Red
Red
6.5
7.5
8.0
8.5
9.5
10.5
6.5
7.5
8.0
8.5
9.5
10.5
6.5-8.5
9.5
10.5

Figure 5

Engineering NIR-Sighted Bacteria

Stefanie S. M. Meier[1,‡], Michael Hörzing[1,‡], Cornelia Böhm[2,3,‡], Emma L. R. Düthorn[1,‡], Heikki Takala[2,‡], René Uebe[4,5,‡], Andreas Möglich[1,5,6,*,‡]

[1] Department of Biochemistry, University of Bayreuth, 95447 Bayreuth, Germany.
[2] Department of Biological and Environmental Science, Nanoscience Center, University of Jyvaskyla, Jyvaskyla 40014, Finland.
[3] Institute of Biochemistry, Graz University of Technology, 8010 Graz, Austria
[4] Department of Microbiology, University of Bayreuth, 95447 Bayreuth, Germany.
[5] Bayreuth Center for Biochemistry & Molecular Biology, Universität Bayreuth, 95447 Bayreuth, Germany.
[6] North-Bavarian NMR Center, Universität Bayreuth, 95447 Bayreuth, Germany.

* for correspondence: andreas.moeglich@uni-bayreuth.de
‡ ORCID identifiers: S.S.M.M. 0009-0002-6028-5223; M.H. 0009-0008-2301-3783; C.B. 0000-0002-3552-2349; E.L.R.D. 0009-0000-4156-5428; H.T. 0000-0003-2518-8583; R.U. 0000-0003-2357-1589; A.M. 0000-0002-7382-2772

Contents

Supplementary Figure 1 ____ 3

Supplementary Figure 2 ____ 5

Supplementary Figure 3 ____ 6

Supplementary Figure 4 ____ 7

Supplementary Figure 5 ____ 8

Supplementary Figure 6 ____ 9

Supplementary Figure 7 ____ 10

Supplementary Figure 8 ____ 11

Supplementary Figure 9 ____ 12

Supplementary Figure 10 ____ 13

Supplementary Table 1 ____ 14

Supplementary Table 2 ____ 21

Supplementary Figure 1

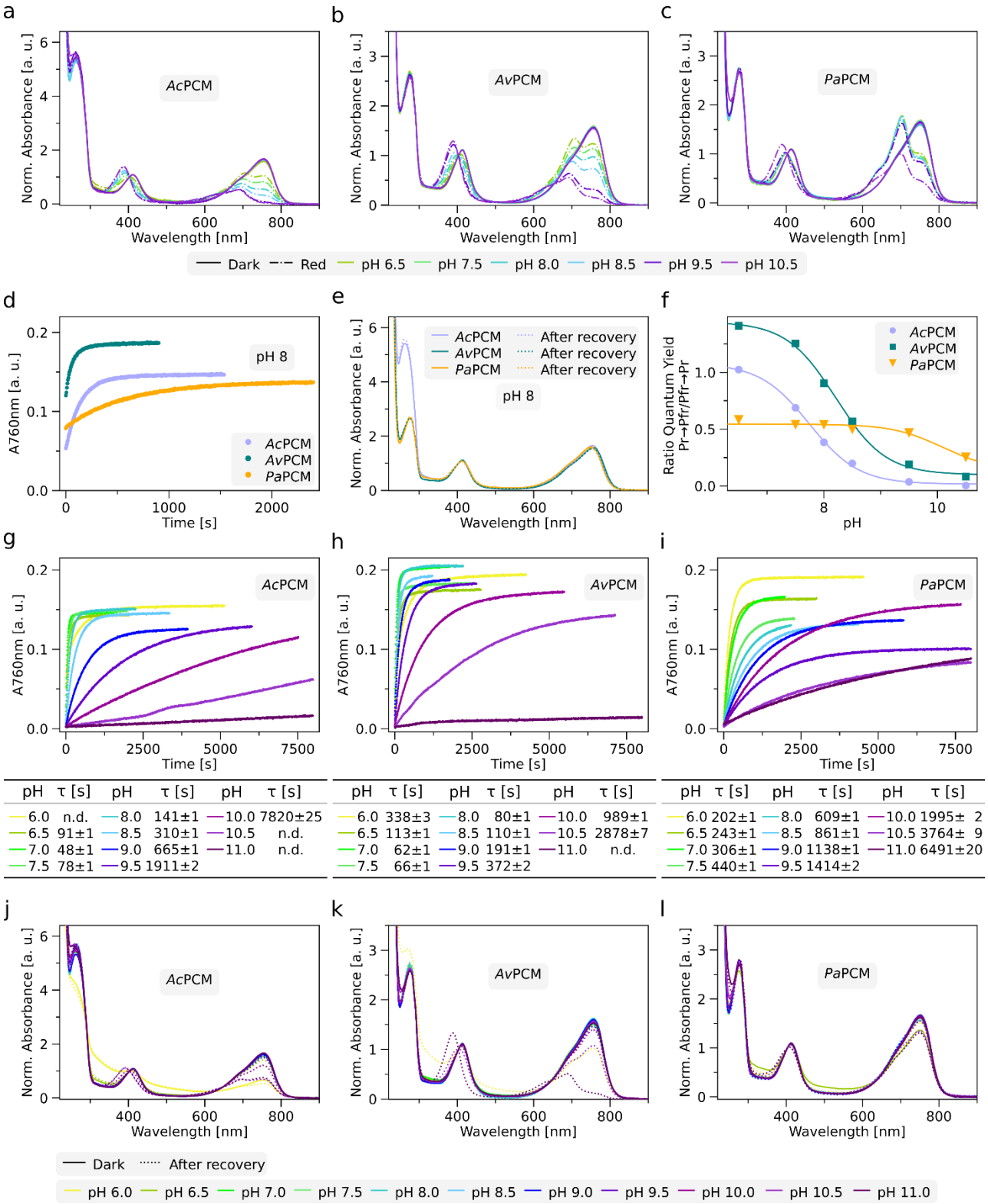

pH	τ [s]	pH	τ [s]	pH	τ [s]
6.0	n.d.	8.0	141±1	10.0	7820±25
6.5	91±1	8.5	310±1	10.5	n.d.
7.0	48±1	9.0	665±1	11.0	n.d.
7.5	78±1	9.5	1911±2		

pH	τ [s]	pH	τ [s]	pH	τ [s]
6.0	338±3	8.0	80±1	10.0	989±1
6.5	113±1	8.5	110±1	10.5	2878±7
7.0	62±1	9.0	191±1	11.0	n.d.
7.5	66±1	9.5	372±2		

pH	τ [s]	pH	τ [s]	pH	τ [s]
6.0	202±1	8.0	609±1	10.0	1995± 2
6.5	243±1	8.5	861±1	10.5	3764± 9
7.0	306±1	9.0	1138±1	11.0	6491±20
7.5	440±1	9.5	1414±2		

Additional spectroscopic characterization of bacteriophytochrome photosensory core modules (PCM) from *Azorhizobium caulinodans* (*Ac*PCM), *Agrobacterium vitis* (*Av*PCM), and *Pseudomonas aeruginosa* (*Pa*PCM). (a) Absorbance spectra of *Ac*PCM at different pH values as indicated below the

graph in darkness (solid line) and after red-light-illumination (dotted line). Data are normalized by the absorbance at 403 nm within the Soret band. (b) and (c) as in (a) but for *Av*PCM and *Pa*PCM. (d) Dark-recovery kinetics of *Ac*PCM (light purple circles), *Av*PCM (dark green circles), and *Pa*PCM (orange circles) monitored at 760 nm, 25°C, and pH 8 after illumination with red light. Time constants determined by single-exponential fits are (147 ± 1) s, (71 ± 1) s and (599 ± 2) s for *Ac*PCM, *Av*PCM, and *Pa*PCM, respectively. (e) Absorbance spectra recorded in darkness (solid lines) and after dark recovery (dotted lines) for *Ac*PCM (light purple), *Av*PCM (dark green), and *Pa*PCM (orange) at pH 8. (f) Ratio of the quantum yields for Pr→Pfr over Pfr→Pr photoconversion as a function of pH. (g) Dark-recovery kinetics of *Ac*PCM recorded at 760 nm after illuminating with NIR light at 25°C and different pH as indicated below the graph. Time constants were determined by single-exponential fits, with the results shown in the table. (h) and (i) as in (g) but for *Av*PCM and *Pa*PCM. (j) Absorbance spectra of *Ac*PCM recorded in darkness (solid lines) and after dark recovery (dotted lines) at different pH as indicated below the graph. (k) and (l) as in (j) but for *Av*PCM and *Pa*PCM.

Supplementary Figure 2

```
                                                PCM                                  Linker FixL
                                                                                    |
DmREDusk    TPRASFSSYVEAVRGVAQPWQAGDLDAALDLRGALLEVQGARLLQELQSELVHVSRLSAM  527
AcNIRusk-0  TPRKSFAIWKETVEHQSWPWTQADRDFAEAARNALVEIVLRHNLQELQSELVHVSRLSAM  518
AvNIRusk-0  TPRKSFAIWKEAVTKQSDHWSENDREVAEAIRAVTVKVVLRHNLQELQSELVHVSRLSAM  516
            *** **: : *:*   :  *   * : *   * . :::   : *****************
                    ▼
DmREDusk    GEMASALAHELNQPLAAISNYMKGSRRLLAGSSDPNTPKVESALDRAAEQALRAGQIIRR  587
AcNIRusk-0  GEMASALAHELNQPLAAISNYMKGSRRLLAGSSDPNTPKVESALDRAAEQALRAGQIIRR  578
AvNIRusk-0  GEMASALAHELNQPLAAISNYMKGSRRLLAGSSDPNTPKVESALDRAAEQALRAGQIIRR  576
            ************************************************************
                        |
                        FixL
```

Multiple sequence alignment of the sensor histidine kinases within *Dm*REDusk, *Ac*NIRusk+0, and *Av*NIRusk+0. The different shading marks the fusion of the photosensory core modules (PCM) of the bacteriophytochromes from *Deinococcus maricopensis* (*Dm*PCM), *Azorhizobium caulinodans* (*Ac*PCM), and *Agrobacterium vitis* (*Av*PCM) with the catalytic domains of the sensor histidine kinase FixL from *Bradyrhizobium japonicum*. The linker region is shown in pink, and the active-site histidine is marked with a red triangle.

Supplementary Figure 3

a

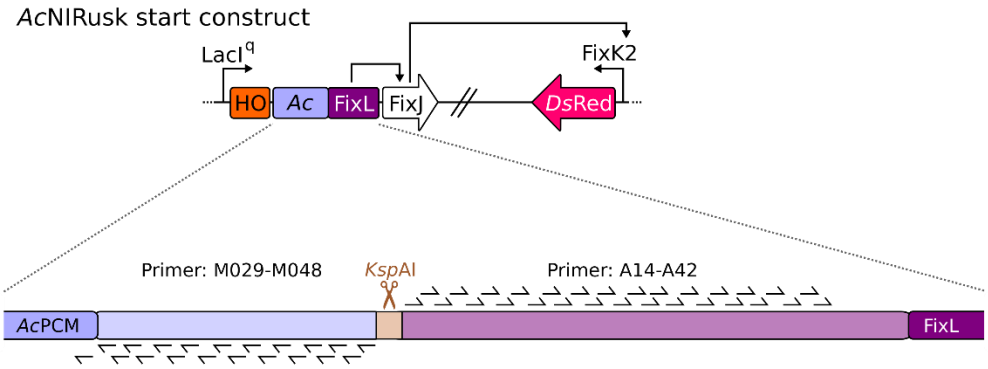

Plasmid	Label	501	257	291	Expression
MH013	sc	VLRHN ELLADERGKADVRQRLLNE	TEHQQTQARLQELQSELVHVSRLSAMGEMASALA	HELN	No
MH021	−4	VLRHN ELLADERG	RLSAMGEMASALA	HELN	NIR/Red
MH019	−1a	VLRHN ELLAD	ELVHVSRLSAMGEMASALA	HELN	NIR
MH034	−1b	VLRHN ELL	QSELVHVSRLSAMGEMASALA	HELN	NIR/Red
MH005	0	VLRHN	LQELQSELVHVSRLSAMGEMASALA	HELN	Dark/NIR/Red
MH017	+16a	VLRHN ELLADER	TEHQQTQARLQELQSELVHVSRLSAMGEMASALA	HELN	Dark/Red
MH018	+16b	VLRHN ELLADERG	EHQQTQARLQELQSELVHVSRLSAMGEMASALA	HELN	Dark

b

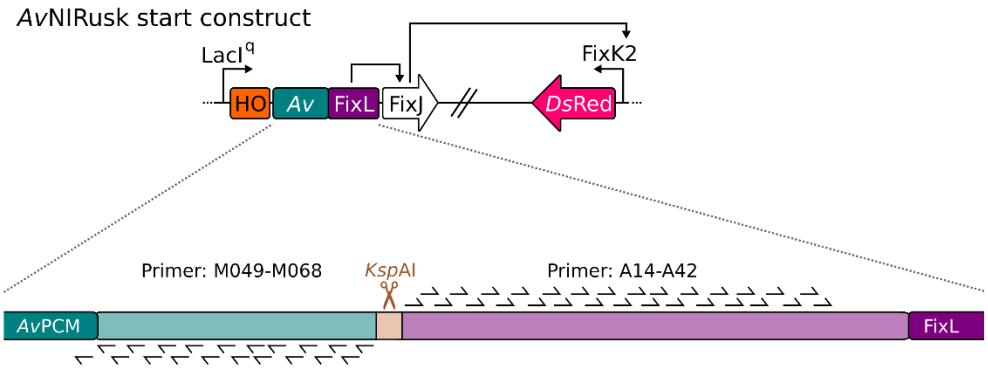

Plasmid	Label	499	257	291	Expression
MH014	sc	VLRHN ELMQEERNKADIRQRVLNE	TEHQQTQARLQELQSELVHVSRLSAMGEMASALA	HELN	No
MH030	−5	VLRHN ELMQEER	RLSAMGEMASALA	HELN	NIR/Red
MH023	−1	VLRHN ELMQE	ELVHVSRLSAMGEMASALA	HELN	NIR
MH006	0	VLRHN	LQELQSELVHVSRLSAMGEMASALA	HELN	Dark/NIR/Red
MH029	+16a	VLRHN ELMQEERN	EHQQTQARLQELQSELVHVSRLSAMGEMASALA	HELN	Dark/Red
MH020	+16b	VLRHN ELMQEER	TEHQQTQARLQELQSELVHVSRLSAMGEMASALA	HELN	Dark/Red
MH028	+17a	VLRHN ELMQEER<u>K</u>	TEHQQTQARLQELQSELVHVSRLSAMGEMASALA	HELN	NIR
MH038	+17b	VLRHN ELMQEERN	TEHQQTQARLQELQSELVHVSRLSAMGEMASALA	HELN	NIR/Red

*Ac*NIRusk (a) and *Av*NIRusk (b) PATCHY start constructs (sc) and derived linker variants. The linker between the *Ac*/*Av*PCM and FixL was adopted from the parental proteins and is defined as the region between the PCM (residues VLRHN) and the active-site histidine at position 291. At the junction, a *Ksp*AI restriction site and a frameshift were inserted. Underlined amino acids originate from a cloning artifact. PATCHY primers are listed in Suppl. Table 1.

Supplementary Figure 4

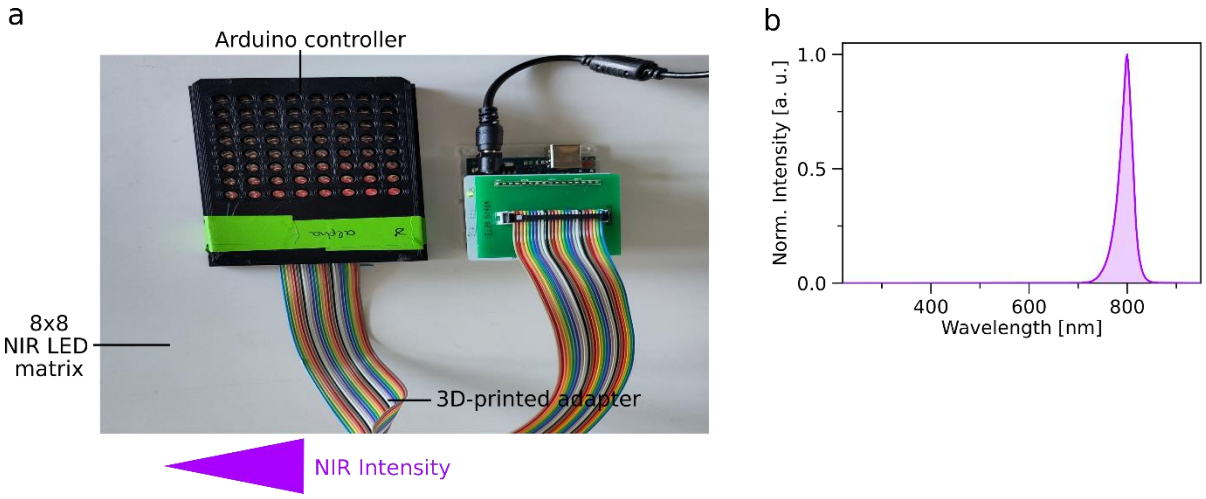

Setup for illumination with near-infrared (NIR) light at different intensities in a microtiter-plate (MTP) format. (a) The programmable 8-by-8 matrix of NIR light-emitting diodes (LED) is based on a previous setup (Hennemann et al., 2018; Stüven et al., 2019) and integrated into a 3D-printed adapter. NIR-light intensities can be adjusted by an Arduino microcontroller. (b) Emission spectrum of the NIR LED matrix with a maximum at 800 nm and a full width at half-maximum of 18 nm.

Supplementary Figure 5

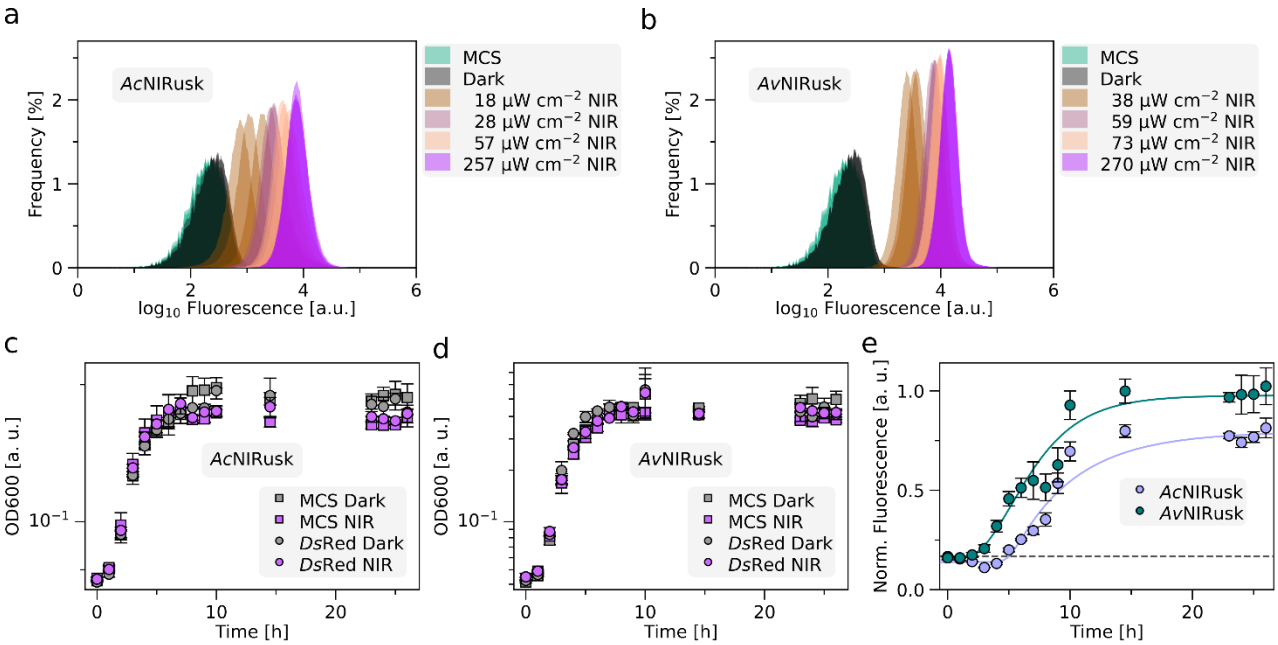

(a-b) Analyses by flow cytometry of *Ds*Red production in bacteria containing *Ac*NIRusk (a) or *Av*NIRusk (b) when incubated in darkness (black), or under different NIR-light intensities. An empty-vector control (MCS) is shown in green. (c) Growth kinetics of bacteria bearing *Ac*NIRusk-*Ds*Red (circles) or empty-vector controls (MCS, squares) in darkness (gray) or NIR light (purple). (d) as in (c) but for *Av*NIRusk. (e) *Ds*Red production induced by NIR light in bacteria containing *Ac*NIRusk (light purple circles) or *Av*NIRusk (dark green circles) over time. The background fluorescence of bacteria carrying the empty-vector control is indicated by the dashed line. Fluorescence readings are normalized as in Fig. 2b. Data were fitted by logistic functions.

Supplementary Figure 6

a

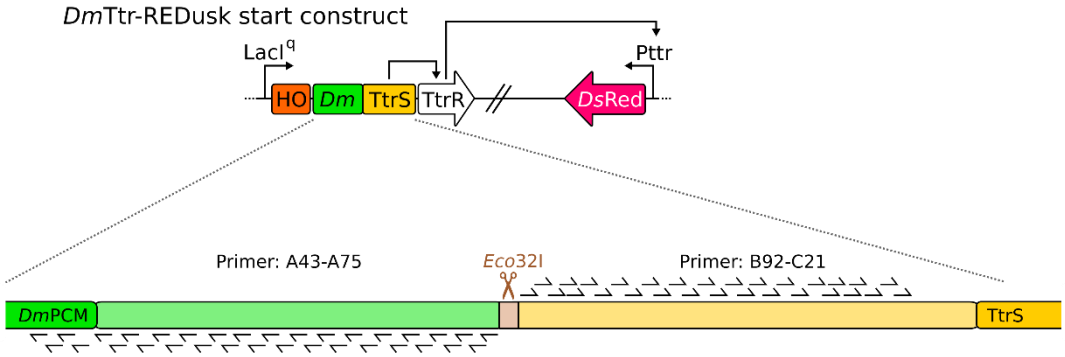

Plasmid	Label	510 … 407 … 441	Expression
SM123	sc	GARL AALQDLNARLERANRELEGRNAELRRFAF RELINTQRQLNENRALLEHAQRIAIAGELGASLS HELN	No
SM146	−13	GARL A AIAGELGASLS HELN	Red
SM147	0	GARL LNENRALLEHAQRIAIAGELGASLS HELN	Dark/NIR
SM148	+5	GARL AA QRQLNENRALLEHAQRIAIAGELGASLS HELN	Red
SM149	+7a	GARL A INTQRQLNENRALLEHAQRIAIAGELGASLS HELN	Dark/NIR
SM150	+7b	GARL AALQDLNARLERANRELEGRNAELRR LGASLS HELN	Dark/NIR
SM153	+14	GARL AALQDLNARLERANRELEGRNAELRRFAFD AGELGASLS HELN	Dark/NIR

b

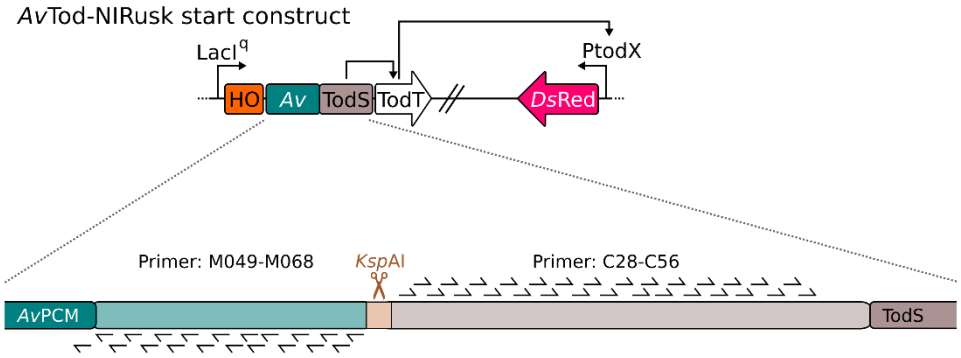

Plasmid	Label	499 … 726 … 760	Expression
SM128	sc	VLRHN ELMQEERNKADIRQRVLNE TEKKQAQENLNQLQQQLVYVSRSATMGEFAAYIA HEIN	No
SM160	+3	VLRHN ELMQEERNKADIRQRVLNE MGEFAAYIA HEIN	NIR
SM161	+16	VLRHN ELMQEERNKADIRQRVLNEV QQQLVYVSRSATMGEFAAYIA HEIN	Dark/Red
SM162	+19	VLRHN ELMQEERNKADIRQRVLNEV NQLQQQLVYVSRSATMGEFAAYIA HEIN	Dark
SM163	+21	VLRHN ELMQEERNKADIRQR KQAQENLNQLQQQLVYVSRSATMGEFAAYIA HEIN	NIR/Red
SM164	+26	VLRHN ELMQEERNKADIRQRVL TEKKQAQENLNQLQQQLVYVSRSATMGEFAAYIA HEIN	Dark/Red

*Dm*Ttr-REDusk (a) and *Av*Tod-NIRusk (b) PATCHY start constructs (sc) and derived linker variants. The linker between the *Dm*/*Av*PCM and the TtrS/TodS two-component system was adopted from the natural proteins. At the junction, a *Eco*32I or *Ksp*AI restriction site and a frameshift were inserted. Underlined amino acids highlighted derive from a cloning artifact. PATCHY primers are listed in Suppl. Table 1.

Supplementary Figure 7

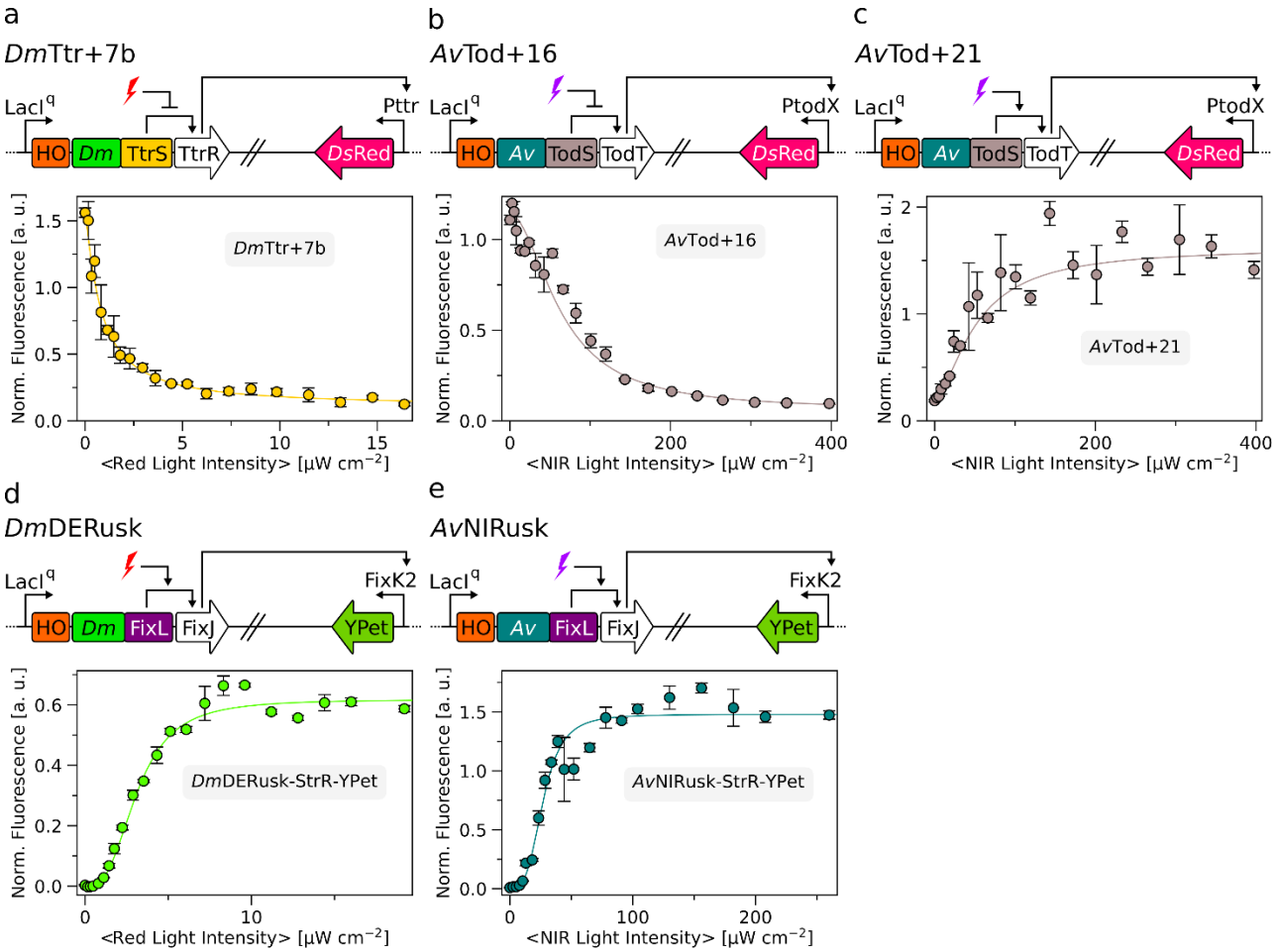

f

	Dark	NIR	Red	NIR+Red
*Dm*Ttr+7b-*Ds*Red + *Dm*DERusk-YPet	DsRed	DsRed	YPet	YPet
*Av*Tod+21-*Ds*Red + *Dm*DERusk-YPet		DsRed	YPet	YPet
*Av*Tod+16-*Ds*Red + *Dm*DERusk-YPet	DsRed		DsRed, YPet	YPet
*Av*Tod+16-*Ds*Red + *Av*NIRusk-YPet	DsRed	YPet	DsRed	

Characterization of constructs used in multiplexing experiments. (a) Schematic of *Dm*Ttr+7b (top) and associated light-dose response (bottom). (b) and (c) as in (a) but for *Av*Tod+16 and *Av*Tod+21. Data in panels a-c are normalized as in Fig. 2. (d) Schematic of *Dm*DERusk-StrR-YPet (top) and the associated light-dose response (bottom). (e) as in (d) but for *Av*NIRusk-StrR-YPet. Data in panels d-f are normalized as in Fig. 3. (f) The schematic summarizes the results of the multiplexing experiments from Fig. 3c. The production of *Ds*Red and YPet under different light conditions are shown by pink pentagons and green heptagons, respectively.

Supplementary Figure 8

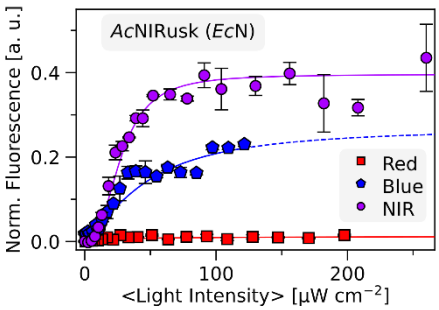

Light-regulated gene expression in *Escherichia coli* Nissle (*Ec*N) containing *Ac*NIRusk after incubation at varying NIR-light (purple circles), red-light (red squares), and blue-light (blue pentagons) intensities.

Supplementary Figure 9

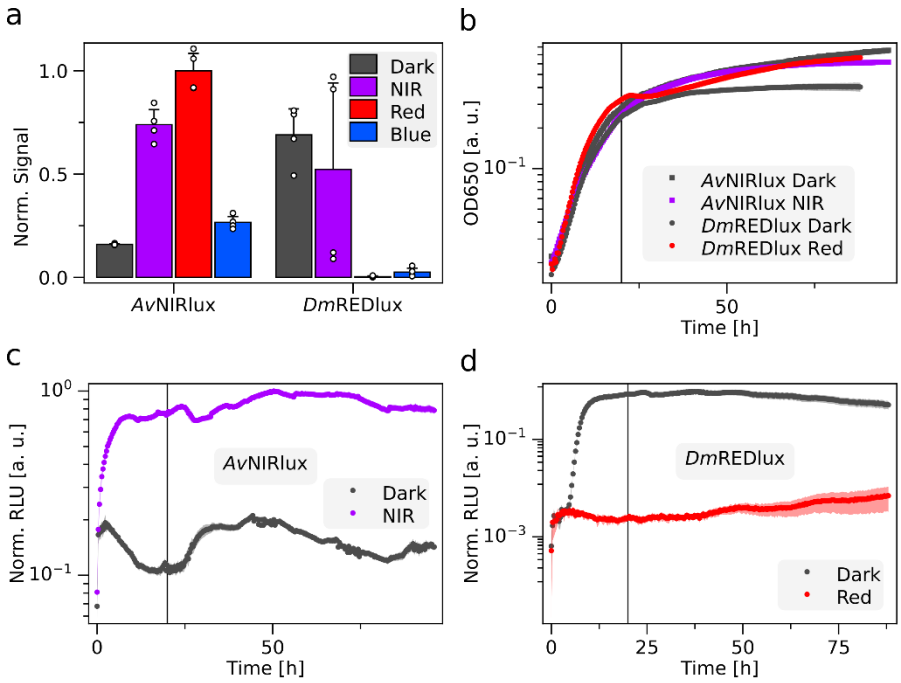

Gene expression regulated by *Av*NIRlux and *Dm*REDlux in *Agrobacterium tumefaciens*. (a) Quantified luminescence from the spotting assay in Fig. 4b. Bar colors represent incubation in darkness (gray), NIR (purple), red (red), or blue (blue) light. (b) Optical density at 650 nm of *A. tumefaciens* bacteria bearing *Av*NIRlux or *Dm*REDlux grown in liquid culture under different light conditions. (c) Normalized reporter luminescence of the bacteria from panel (b) harboring *Av*NIRlux and grown in darkness (grey) or under NIR light (purple). The vertical black line denotes a time point of 20 h on which the data in Fig. 4d are based. (d) as for (c) but for *A. tumefaciens* bacteria containing *Dm*REDlux and illumination with red instead of NIR light (red).

Supplementary Figure 10

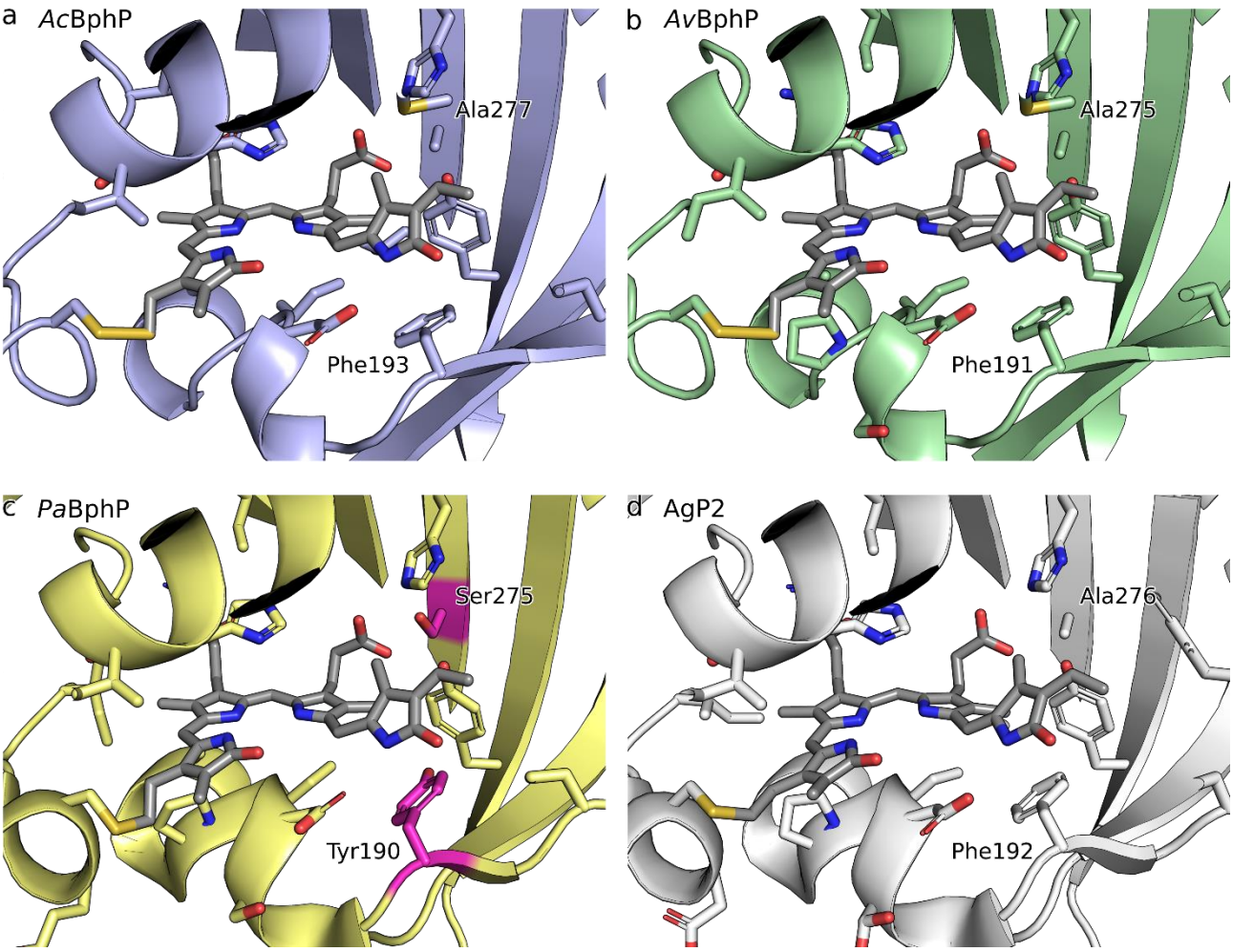

Biliverdin binding pocket in the photosensory core modules (PCM) of (a) *Azorhizobium caulinodans* bacteriophytochrome (BphP), (b) *Agrobacterium vitis* BphP, (c) *Pseudomonas aerugionsa* BphP, and (d) *Agrobacterium tumefaciens* Agp2 BphP. Whereas experimental structures are available for the PCMs of AgP2 [PDB entry 6g1y (Schmidt et al., 2018)] and *Pa*BphP [3c2w (Yang et al., 2008)], for *Ac*BphP and *Av*BphP, PCM models were calculated with AlphaFold3 (Abramson et al., 2024). Tyrosine 190 and serine 275 are highlighted in the *Pa*PCM structure by magenta color. The other three PCMs feature less polar phenylalanine and alanine residues, respectively, in the structurally equivalent positions.

Supplementary Table 1

Oligonucleotides used in this study. Overhang regions are indicated in bold, and restriction enzyme recognition sites are underlined.

Name	Sequence 5'-3'
Primers for cloning of bathy-PCM expression constructs	
M001_Ac_Bb_for	CCTGGTTGAAATTGTGCTGCGTCATAATGAGAATCTTTATTTTCAGCATCACCA
M002_Ac_Bb_rev	GATCAACTGCTTCTGCATTCGGCATGGTATATCTCCTTATTAAAGTTAAACAAAA
M003_Ac_Ins_for	TTTTGTTTAACTTTAATAAGGAGATATACCATGCCGAATGCAGAAGCAGTTGATC
M004_Ac_Ins_rev	TGGTGATGCTGAAAATAAAGATTCTCATTATGACGCAGCACAATTTCAACCAGG
M005_Av_Bb_for	ACCGTTAAAGTGGTTCTGCGCCATAATGAGAATCTTTATTTTCAGCATCACCA
M006_Av_Bb_rev	ATCAACGGTCTGGGTTGCAGGCATGGTATATCTCCTTATTAAAGTTAAACAAAA
M007_Av_Ins_for	TTTTGTTTAACTTTAATAAGGAGATATACCATGCCTGCAACCCAGACCGTTGAT
M008_Av_Ins_rev	TGGTGATGCTGAAAATAAAGATTCTCATTATGGCGCAGAACCACTTTAACGGT
M069_Pa-Ins-fw	TTTTGTTTAACTTTAATAAGGAGATATACCATGACGAGCATCACCCCGGTTACCC
M070_Pa-Ins-rev	TGGTGATGGCCCTGAAAATAAAGATTCTCCGCATGGTTGAGGCACAGTTCCATC
M071_Pa-Bb-fw	GATGGAACTGTGCCTCAACCATGCGGAGAATCTTTATTTTCAGGGCCATCACCA
M072_Pa-Bb-rev	GGGTAACCGGGGTGATGCTCGTCATGGTATATCTCCTTATTAAAGTTAAACAAAA
M017_AcAv_TEVrepair_fw	GGCCATCACCATCACCATCACCATCAC
M018_Ac_TEVrepair_rev	CTGAAAATAAAGATTCTCATTATGACGC
M019_Av_TEVrepair_rev	CTGAAAATAAAGATTCTCATTATGGCGC
Primers for Gibson cloning of bathy-PCMs into pREDusk	
M009_Ac_Bb_for	CCTGGTTGAAATTGTGCTGCGTCATAATCTCCAGGAACTGCAATCCGAGCTCGTC
M010_Ac_Bb_rev	TTGTCAGATCAACTGCTTCTGCATTCGTCATGCGTGGGCGACCTCAGGC
M011_Ac_Ins_for	GCCTGAGGTCGCCCACGCATGACGAATGCAGAAGCAGTTGATCTGACAA
M012_Ac_Ins_rev	GACGAGCTCGGATTGCAGTTCCTGGAGATTATGACGCAGCACAATTTCAACC

	AGG
M013_Av_Bb_for	CCGTTAAAGTGGTTCTGCGCCATAATCTCCAGGAACTGCAATCCGAGCTCGTC
M014_Av_Bb_rev	GTCAGATCAACGGTCTGGGTTGCAGTCATGCGTGGGCGACCTCAGGC
M015_Av_Ins_for	GCCTGAGGTCGCCCACGCATGACTGCAACCCAGACCGTTGATCTGAC
M016_Av_Ins_rev	GACGAGCTCGGATTGCAGTTCCTGGAGATTATGGCGCAGAACCACTTTAACGG
Primers for cloning of PATCHY *Ac*/*Av*NIRusk start constructs	
A07_P_I_II_Step1_for	TTAACCGAGCATCAGCAGACACAAGCACGTCTCCAGGAACTGCAATCCGAGCTCG
M020_AcREDusk_PATCHY_rev1	CGCTCGTCAGCCAGTAATTCATTATGACGCAGCACAATTTCAACC
M021_AcREDusk_PATCHY_rev2	GACGCACGTCTGCTTTCCCGCGCTCGTCAGCCAGTAATTCATTAT
M022_AcREDusk_PATCHY_fw2	AGCGTCTTCTTAATGAAGTTAACCGAGCATCAGCAGACACAAG
M023_AvREDusk_PATCHY_rev1	CGCTCCTCTTGCATCAGTTCATTATGGCGCAGAACCACTTTAACG
M025_AvREDusk_PATCHY_fw2	AGCGTGTCTTAAACGAGGTTAACCGAGCATCAGCAGACACAAG
M028_AvREDusk_PATCHY_rev2	GACGAATGTCTGCTTTGTTACGCTCCTCTTGCATCAGTTCATTAT
PATCHY forward primers for amplification of FixL	
A14_P_I_II_for_1	ACCGAGCATCAGCAGAC
A15_P_I_II_for_2	GAGCATCAGCAGACACAAG
A16_P_I_II_for_3	CATCAGCAGACACAAGC
A17_P_I_II_for_4	CAGCAGACACAAGCACG
A18_P_I_II_for_5	CAGACACAAGCACGTCTC
A19_P_I_II_for_6	ACACAAGCACGTCTCC
A20_P_I_II_for_7	CAAGCACGTCTCCAGG
A21_P_I_II_for_8	GCACGTCTCCAGGAAC
A22_P_I_II_for_9	CGTCTCCAGGAACTGC
A23_P_I_II_for_10	CTCCAGGAACTGCAATCC
A24_P_I_II_for_11	CAGGAACTGCAATCCG
A25_P_I_II_for_12	GAACTGCAATCCGAGC
A26_P_I_II_for_13	CTGCAATCCGAGCTCG
A27_P_I_II_for_14	CAATCCGAGCTCGTCC
A28_P_I_II_for_15	TCCGAGCTCGTCCACG

A29_P_I_II_for_16	GAGCTCGTCCACGTCTC
A30_P_I_II_for_17	CTCGTCCACGTCTCCAG
A31_P_I_II_for_18	GTCCACGTCTCCAGGC
A32_P_I_II_for_19	CACGTCTCCAGGCTGAG
A33_P_I_II_for_20	GTCTCCAGGCTGAGCG
A34_P_I_II_for_21	TCCAGGCTGAGCGCCATG
A35_P_I_II_for_22	AGGCTGAGCGCCATGG
A36_P_I_II_for_23	CTGAGCGCCATGGGCG
A37_P_I_II_for_24	AGCGCCATGGGCGAAATG
A38_P_I_II_for_25	GCCATGGGCGAAATGG
A39_P_I_II_for_26	ATGGGCGAAATGGCGTC
A40_P_I_II_for_27	GGCGAAATGGCGTCCG
A41_P_I_II_for_28	GAAATGGCGTCCGCGC
A42_P_I_II_for_29	ATGGCGTCCGCGCTCG
PATCHY forward primers for amplification of TtrS	
B92_P_Ttr_for_01	CGCGAACTGATTAATACCC
B93_P_Ttr_for_02	GAACTGATTAATACCCAGCG
B94_P_Ttr_for_03	CTGATTAATACCCAGCGTCAG
B95_P_Ttr_for_04	ATTAATACCCAGCGTCAGC
B96_P_Ttr_for_05	AATACCCAGCGTCAGC
B97_P_Ttr_for_06	ACCCAGCGTCAGCTGAATG
B98_P_Ttr_for_07	CAGCGTCAGCTGAATG
B99_P_Ttr_for_08	CGTCAGCTGAATGAAAATCG
C01_P_Ttr_for_09	CAGCTGAATGAAAATCGTG
C02_P_Ttr_for_10	CTGAATGAAAATCGTGCACTG
C03_P_Ttr_for_11	AATGAAAATCGTGCACTGC
C04_P_Ttr_for_12	GAAAATCGTGCACTGCTG
C05_P_Ttr_for_13	AATCGTGCACTGCTGG
C06_P_Ttr_for_14	CGTGCACTGCTGGAAC
C07_P_Ttr_for_15	GCACTGCTGGAACATGC
C08_P_Ttr_for_16	CTGCTGGAACATGCACAG
C09_P_Ttr_for_17	CTGGAACATGCACAGC
C10_P_Ttr_for_18	GAACATGCACAGCGTATTG
C11_P_Ttr_for_19	CATGCACAGCGTATTGC
C12_P_Ttr_for_20	GCACAGCGTATTGCCATTG

C13_P_Ttr_for_21	CAGCGTATTGCCATTGC
C14_P_Ttr_for_22	CGTATTGCCATTGCCG
C15_P_Ttr_for_23	ATTGCCATTGCCGGTG
C16_P_Ttr_for_24	GCCATTGCCGGTGAAC
C17_P_Ttr_for_25	ATTGCCGGTGAACTGG
C18_P_Ttr_for_26	GCCGGTGAACTGGGTG
C19_P_Ttr_for_27	GGTGAACTGGGTGCAAG
C20_P_Ttr_for_28	GAACTGGGTGCAAGCC
C21_P_Ttr_for_29	CTGGGTGCAAGCCTGAG
PATCHY forward primers for amplification of TodS	
C28_P_Tod_for_01	ACTGAGAAGAAACAAGCACAGG
C29_P_Tod_for_02	GAGAAGAAACAAGCACAGG
C30_P_Tod_for_03	AAGAAACAAGCACAGGAAAATC
C31_P_Tod_for_04	AAACAAGCACAGGAAAATCTTAACC
C32_P_Tod_for_05	CAAGCACAGGAAAATCTTAACC
C33_P_Tod_for_06	GCACAGGAAAATCTTAACCAG
C34_P_Tod_for_07	CAGGAAAATCTTAACCAGTTGC
C35_P_Tod_for_08	GAAAATCTTAACCAGTTGCAGC
C36_P_Tod_for_09	AATCTTAACCAGTTGCAGCAAC
C37_P_Tod_for_10	CTTAACCAGTTGCAGCAACAAC
C38_P_Tod_for_11	AACCAGTTGCAGCAACAAC
C39_P_Tod_for_12	CAGTTGCAGCAACAACTTG
C40_P_Tod_for_13	TTGCAGCAACAACTTGTG
C41_P_Tod_for_14	CAGCAACAACTTGTGTACG
C42_P_Tod_for_15	CAACAACTTGTGTACGTTTCC
C43_P_Tod_for_16	CAACTTGTGTACGTTTCCC
C44_P_Tod_for_17	CTTGTGTACGTTTCCCGATC
C45_P_Tod_for_18	GTGTACGTTTCCCGATCAG
C46_P_Tod_for_19	TACGTTTCCCGATCAGC
C47_P_Tod_for_20	GTTTCCCGATCAGCTACG
C48_P_Tod_for_21	TCCCGATCAGCTACGATG
C49_P_Tod_for_22	CGATCAGCTACGATGGG
C50_P_Tod_for_23	TCAGCTACGATGGGTGAATTTG
C51_P_Tod_for_24	GCTACGATGGGTGAATTTG
C52_P_Tod_for_25	ACGATGGGTGAATTTGC

C53_P_Tod_for_26	ATGGGTGAATTTGCAGC
C54_P_Tod_for_27	GGTGAATTTGCAGCCTATATTG
C55_P_Tod_for_28	GAATTTGCAGCCTATATTGC
C56_P_Tod_for_29	TTTGCAGCCTATATTGCACAC
PATCHY reverse primers for amplification of *Ac*PCM	
M029_Ac_rev1	TTCATTAAGAAGACGCTGACG
M030_Ac_rev2	ATTAAGAAGACGCTGACGC
M031_Ac_rev3	AAGAAGACGCTGACGC
M032_Ac_rev4	AAGACGCTGACGCACG
M033_Ac_rev5	ACGCTGACGCACGTCTG
M034_Ac_rev6	CTGACGCACGTCTGCTTTC
M035_Ac_rev7	ACGCACGTCTGCTTTCC
M036_Ac_rev8	CACGTCTGCTTTCCCG
M037_Ac_rev9	GTCTGCTTTCCCGCGC
M038_Ac_rev10	TGCTTTCCCGCGCTCG
M039_Ac_rev11	TTTCCCGCGCTCGTCAG
M040_Ac_rev12	CCCGCGCTCGTCAGCC
M041_Ac_rev13	GCGCTCGTCAGCCAGTAATTC
M042_Ac_rev14	CTCGTCAGCCAGTAATTCATTATG
M043_Ac_rev15	GTCAGCCAGTAATTCATTATGACG
M044_Ac_rev16	AGCCAGTAATTCATTATGACG
M045_Ac_rev17	CAGTAATTCATTATGACGCAGC
M046_Ac_rev18	TAATTCATTATGACGCAGCAC
M047_Ac_rev19	TTCATTATGACGCAGCAC
M048_Ac_rev20	ATTATGACGCAGCACAATTTC
PATCHY reverse primers for amplification of *Av*PCM	
M049_Av_rev1	CTCGTTTAAGACACGCTGAC
M050_Av_rev2	GTTTAAGACACGCTGACGAATG
M051_Av_rev3	TAAGACACGCTGACGAATG
M052_Av_rev4	GACACGCTGACGAATGTC
M053_Av_rev5	ACGCTGACGAATGTCTGC
M054_Av_rev6	CTGACGAATGTCTGCTTTG
M055_Av_rev7	ACGAATGTCTGCTTTGTTACG
M056_Av_rev8	AATGTCTGCTTTGTTACGC
M057_Av_rev9	GTCTGCTTTGTTACGCTCC

M058_Av_rev10	TGCTTTGTTACGCTCCTC
M059_Av_rev11	TTTGTTACGCTCCTCTTGC
M060_Av_rev12	GTTACGCTCCTCTTGCATC
M061_Av_rev13	ACGCTCCTCTTGCATCAG
M062_Av_rev14	CTCCTCTTGCATCAGTTCATTATG
M063_Av_rev15	CTCTTGCATCAGTTCATTATGG
M064_Av_rev16	TTGCATCAGTTCATTATGGC
M065_Av_rev17	CATCAGTTCATTATGGCGC
M066_Av_rev18	CAGTTCATTATGGCGCAG
M067_Av_rev19	TTCATTATGGCGCAGAACC
M068_Av_rev20	ATTATGGCGCAGAACC
Primers for cloning of orthogonal TtrSR TCS	
B55_Pttr_BglII_for	CGTTAAAGATCTATATTTGTTGCGCTAGA
B56_Pttr_XbaI_rev	TGCCAGTCTAGAACAGGCATTC
B57_Bb_for_DmTtrSR	ACGTCTGCGTCTGGAAGATAATCGTTAACAATTGATGTAAGTTAGCTCACTCA
B58_Bb_rev_DmTtrSR	CATTCAGCTGACGCTGGGTATTAATCAGCTCACGATTAGCACGCTCTAAG
B59_Ins_for_DmTtrSR	CTTAGAGCGTGCTAATCGTGAGCTGATTAATACCCAGCGTCAGCTGAATG
B60_Ins_rev_DmTtrSR	TGAGTGAGCTAACTTACATCAATTGTTAACGATTATCTTCCAGACGCAGACGT
B84_P_V_sc_for	GGCGTTTCGCCTTTGATATCGCGAACTGATTAATACCCAGCGTCAG
B85_P_V_sc_rev	GCAACTCTGCGTTACGCCCTTCAAGCTCACGATTAGCACGCTCTA
Primers for cloning of orthogonal TodST TCS	
TodX_fw	GCACAAGATCTGGTCTGAGGTTTTCATCGAC
TodX_rv	CGTGCTCTAGAAATTACAATCCTTCCAC
0_pDusk_fw	GAGTCAATTGAGGGTGGTGAATGTGGCTAG
1_TodS_fw	GATATCACCGAGAAGAAACAAGCACAGGAAAATC
2_NoMfeI_rv	CGTACACAAGTTGTTGCTGCAACTGGTTAAGATTTTCCTGTGCTTGTTTC
3_TodS_fw	GCAGCAACAACTTGTGTACGTTTCCCGATC
4_TodT_rv	GCATCAATTGCTATTCCAGGCTATCCTTGAG
5_pDusk_rv	GCTTGTTTCTTCTCGGTGATATCATTCTGAATTC
M014_Av_Bb_rev	GTCAGATCAACGGTCTGGGTTGCAGTCATGCGTGGGCGACCTCAGGC
M015_Av_Ins_for	GCCTGAGGTCGCCCACGCATGACTGCAACCCAGACCGTTGATCTGAC
C26_Bb_for_P_X_sc	ATTCGTCAGCGTGTCTTAAACGAGGTTAACTGAGAAGAAACAAGCACAG
C27_Ins_rev_P_X_sc	CTGTGCTTGTTTCTTCTCAGTTAACCTCGTTTAAGACACGCTGACGAAT

Primers for cloning StrR variants	
B73_Bb_for_pStrepDusk	GATCACCAAGGTAGTCGGCAAATAAGAATTAATTCATGAGCGGATACATATT
B74_Bb_rev_pStrepDusk	AAGGATCTCAAGAAGATCCTTTGATCTGATGCCTCCGTGTAAGGGG
B75_Ins_for_pStrepDusk	CCCCTTACACGGAGGCATCAGATCAAAGGATCTTCTTGAGATCCTT
B76_Ins_rev_pStrepDusk	AATATGTATCCGCTCATGAATTAATTCTTATTTGCCGACTACCTTGGTGATC
B26_Ins_rev	CGAGATGATAGGAGGTCTAGCATGACGACCAAGGGACATATCTACG
B27_Bb_for	CGTAGATATGTCCCTTGGTCGTCATGCTAGACCTCCTATCATCTCG
M014_Av_Bb_rev	GTCAGATCAACGGTCTGGGTTGCAGTCATGCGTGGGCGACCTCAGGC
M015_Av_Ins_for	GCCTGAGGTCGCCCACGCATGACTGCAACCCAGACCGTTGATCTGAC
Primers for cloning MCS variant	
C76_Bb_for_MCS	ATCAGCAACTACATGAAGGGCTCGCGGCGGCTGCTTGCCG
C77_Ins_rev_MCS	CGGCAAGCAGCCGCCGCGAGCCCTTCATGTAGTTGCTGAT
M014_Av_Bb_rev	GTCAGATCAACGGTCTGGGTTGCAGTCATGCGTGGGCGACCTCAGGC
M015_Av_Ins_for	GCCTGAGGTCGCCCACGCATGACTGCAACCCAGACCGTTGATCTGAC
Primers for cloning lux variants	
lux-op_Nde_for	**GGATCCCATATG** AAATTTGGAAACTTTTTGCTTACATACC
lux-op_Sac_rev	**TGACGAGCTC** TCAACTATCAAACGCTTCG
PfixK2_NdeI_for	**TGACCATATG** ATATCTCCTTCTTAAAGTTAAACAAAATT
PfixK2_rev_OLPmamG	**ACTAAGAGCTAGTAAAGCGAAAAAG** CGGGATCTCGACGCTCTC
DrHo_OLPmamG_for	**CTTTTTCGCTTTACTAGCTCTTAGTTCTCCAATAAATTCCCTGCGAAGCTTAGGAGATCAGTATATG** CTCCGACTCATGATCATGAAGC
FixJ_NotI_rev	**TGACGCGGCCGC** TCAATCGTTGAGCATGCC

Supplementary Table 2

Plasmids used in this study.

Id	Construct	Reference
pBAM2	*p15A* ori, miniTn5, Amp^R, Kan^R	Uebe, unpublished
pBAM2-luxAE	*p15A* ori, miniTn5, Amp^R, Kan^R, *luxABCDE*	(Dziuba et al., 2021)
p*Dm*REDlux	*p15A* ori, miniTn5, Amp^R, Kan^R, PfixK2-*luxABCDE*, PmamDC-*DrhemO-Dmpcm-fixL*	(this study)
p*Av*NIRlux	*p15A* ori, miniTn5, Amp^R, Kan^R, PfixK2-*luxABCDE*, PmamDC-*DrhemO-Avpcm-fixL*	(this study)
pMH005	*Ac*NIRusk-0	(this study)
pMH006	*Av*NIRusk-0	(this study)
pMH008	pCDF-Duet-*Ac*PCM/HO	(this study)
pMH009	pCDF-Duet-*Av*PCM/HO	(this study)
pMH013	*Ac*NIRusk-PATCHY-start construct	(this study)
pMH014	*Av*NIRusk-PATCHY-start construct	(this study)
pMH017	*Ac*NIRusk+16a	(this study)
pMH018	*Ac*NIRusk+16b	(this study)
pMH019	*Ac*NIRusk-1a (*Ac*NIRusk)	(this study)
pMH020	*Av*NIRusk+16b	(this study)
pMH021	*Ac*NIRusk-4	(this study)
pMH023	*Av*NIRusk-1	(this study)
pMH026	pCDF-Duet-*Pa*PCM/HO	(this study)
pMH028	*Av*NIRusk+17a (*Av*NIRusk)	(this study)
pMH029	*Av*NIRusk+16a	(this study)
pMH030	*Av*NIRusk-5	(this study)
pMH034	*Ac*NIRusk-1b	(this study)
pMH038	*Av*NIRusk+17b	(this study)
pMIR66	TodS and TodT proteins	(Ramos-González et al., 2002)
pMIR77	PtodX promoter	(Ramos-González et al., 2002)

pQX037	*Pa*PAC	(Xu et al., 2024)
pQX086	*Av*PAC	(Xu et al., 2024)
pQX091	*Ac*PAC	(Xu et al., 2024)
pRD349	pDusk-YT1-X	(unpublished)
pSM001	*Dr*REDusk-MCS	(Multamäki et al., 2022)
pSM003	*Dm*REDusk	(Meier et al., 2024a)
pSM024	*Dm*REDusk-MCS	(Meier et al., 2024a)
pSM087	*Dm*DERusk	(Meier et al., 2024a)
pSM090	*Dm*DERusk-YPet	(Meier et al., 2024a)
pSM091	*Dm*DERusk-MCS	(Meier et al., 2024a)
pSM122	*Dm*DERusk-StrR-YPet	(this study)
pSM123	*Dm*Ttr-REDusk-PATCHY-start construct	(this study)
pSM128	*Av*Tod-NIRusk PATCHY-start construct	(this study)
pSM136	*Av*NIRusk-StrR-YPet	(this study)
pSM146	*Dm*Ttr-13	(this study)
pSM147	*Dm*Ttr-0	(this study)
pSM148	*Dm*Ttr+5	(this study)
pSM149	*Dm*Ttr+7a	(this study)
pSM150	*Dm*Ttr+7b	(this study)
pSM153	*Dm*Ttr+14	(this study)
pSM160	*Av*Tod+3	(this study)
pSM161	*Av*Tod+16	(this study)
pSM162	*Av*Tod+19	(this study)
pSM163	*Av*Tod+21	(this study)
pSM164	*Av*Tod+26	(this study)
pSM182	*Av*NIRusk-MCS	(this study) Addgene: 235084